This is a preprint, the final version is subject to change, of the American Mineralogist (MSA)
Cite as Authors (Year) Title. American Mineralogist, in press.
DOI: https://doi.org/10.2138/am-2018-6192

Revision 2

The Mantle Source of Thermal Plumes: Trace and Minor Elements in Olivine & Major Oxides of Primitive Liquids (And Why the Olivine Compositions Don't matter)

Keith Putirka [1], Yan Tao [2], K.R. Hari [3], Perfit, M.[4], Jackson, M.G.[5], and Arevalo Jr., R.[6]
[1] California State University, Fresno, Department of Earth and Environmental Sciences, 2576 E. San Ramon Ave., MS/ST25, Fresno, CA 93740, USA
[2] State Key Laboratory of Ore Deposit Geochemistry, Institute of Geochemistry, Chinese Academy of Sciences, Guiyang, 550002, China
[3] School of Studies in Geology and Water Resource Management, Pt. Ravishankar Shukla University, Raipur- 492010, Chhattisgarh, India
[4] Department of Geological Sciences, Box 112120, University of Florida, Gainesville Fl 32611-2120, USA
[5] University of California Santa Barbara, Department of Earth Science, Santa Barbara, CA, 93106-9630, USA
[6] NASA Goddard Space Flight Center, Planetary Environments Lab, Greenbelt, MD 20771

ABSTRACT

We estimate the mantle source compositions for mantle plumes, and by implication Earth's lower mantle, by: (a) measuring trace (e.g, Sc, V, Cu) and minor (e.g., Ca, Mn, Ni) element concentrations of high forsterite olivine grains from several plume localities, (b) estimating the parent liquid compositions from which they crystallized, (c) calculating mantle potential temperatures and degrees of partial melting and (d) estimating trace element compositions of depleted and enriched mantle sources. Our sample set includes two continental flood basalt provinces (Emeishan and Deccan), a flood basalt that erupted in a continental rift setting (Baffin Island), our type example of a thermal mantle plume (Hawaii) and lavas from the Siqueiros Transform at the East Pacific Rise, which represent the mid-ocean ridge system. We also present olivine compositions for the peridotite xenoliths from Kilbourne Hole, New Mexico, USA, which are commonly used as primary and secondary analytical standards. We find that trace elements in lava-hosted olivine grains are too far removed from their mantle source to provided anything but greatly hindered views of such. Olivine compositions reflect not only evolving liquid compositions (including partial melting conditions and later fractionation), but also evolving Ol+liq partition coefficients, which mostly increase with decreasing *T* during crystallization. Mantle compositions, delimited by maximum forsterite contents and estimates of parental magmas (and experimentally determined partition coefficients) indicate that our selected plumes reflect some combination of (1) a depleted mantle source that is quite similar to that obtained by other methods, and (2) a variably enriched plume source that is more enriched than current estimates of pyrolite. The enriched plume mantle sources can be explained remarkably well as a mixture of subducted mid-ocean ridge basalt (MORB; Gale et al. 2013) and depleted MORB mantle (DM; Salters and Stracke 2004), with MORB:DM ratios of 1:5 to 1:4. These ratios are most sensitive to

estimates of melt fraction where plume parental magmas are last equilibrated with their mantle source, but are nonetheless consistent across a wide range of chemically very different elements, and estimates of MORB and DM obtained by very different means. Baffin Island is of particular interest. Like prior studies, we verify a high mantle potential temperature (T_p) of 1630°C (compared to T_p = 1320-1420°C for MORB from Cottrell and Kelley 2011 for Ol of Fo89.3-91.4). The Baffin source is also within error the same as DM with respect to trace elements, although still isotopically distinct; Baffin appears to be sourced in something that is akin to DM that lies at the base of the mantle, where plumes acquire their excess heat. Thus while part of our analysis supports the concept of a "slab graveyard" at the bottom of the lower mantle (e.g., Wyession 1996), that cemetery is by no means ubiquitous at the CMB: subducted slabs are either unevenly interred, or efficiently excavated by later upwellings.

INTRODUCTION

An enduring obscurity concerns the composition and mineralogy of Earth's lower mantle—we may indeed have a better understanding of Pluto's surface (Moore et al. 2016) than Earth's lower reaches. As to the upper mantle, mantle xenoliths are a key source of information, since they are just one step removed (they are often residues of prior melt extraction) from the mantle source that gives rise to basalts (e.g., McDonough and Sun 1995; Salters and Stracke 2004; Workman and Hart 2005). Basalts, if sufficiently primitive, are also just one step removed from a pre-melt extraction mantle, and their compositions have been used to infer, for example, that subducted crust may be admixed into the sources of MORB (Hirschmann and Stolper, 1996; Waters et al. 2011) and ocean island basalts (OIB) (e.g., Hawkesworth et al. 1979; Hofmann and White 1982; Prytulak and Elliott 2007; Jackson et al. 2008). OIB are in turn thought to derive as deep-seated thermal plumes from the core-mantle boundary (Morgan 1972), and so their sources may provide our most direct view of the lower mantle.

Olivine (Ol) phenocrysts have been offered as an additional, perhaps less biased, view of MORB and OIB mantle sources (e.g., Sobolev et al. 2007). One obvious advantage is that primitive Ol grains are highly resistant to the mixing processes that homogenize

magmatic liquids, and so might preserve what is otherwise lost to magma mixing. Clearly, diffusion may later homogenize phenocrysts (Thomson and Maclennan 2013), but the diversity of disequilibrium Ol grains demonstrates that the process is quite incomplete. As a test, we present new analyses of trace (Ti, V, Cr, Cu, etc.) and minor elements (Ni, Ca, Mn, etc.; for simplicity, herein referred to as "trace" elements) in olivine grains from several plume localities, and a MORB from the East Pacific Rise. Our data show that olivine compositions provide a rather opaque view of mantle composition, especially compared to their host lavas. For some elements (Ni and Cr) olivine compositions reveal quite little about mantle source regions (instead recording how their parent magmas were generated, i.e., at high *P* or *T* or high melt fraction), while for others (Sc and Ti, and possibly Ca) signatures of the mantle source(s) may be preserved, but through a connection that is not perfectly clear.

We first review some crucial, perhaps under-appreciated, controls on oceanic volcanic compositions, and how olivine compositions respond to *T* and liquid composition. Our analysis, which includes some new estimates of mantle-equilibrated parental magmas and the mantle potential temperatures at which they were formed, indicate that the lower mantle contains a depleted component similar to depleted MORB mantle, which is herein noted as DMM ["DM" in Stracke and Salters (2004) and "DMM" in Workman and Hart (2005) with further variations in Shimizu et al. 2016]. This finding is tentative to be sure, but not new, as the FOZO component of Hart et al. (1992) has near DMM-like $^{87}Sr/^{86}Sr$ (0.70248) and $^{143}Nd/^{144}Nd$ (0.5131) and so is clearly quite depleted. What remains clear is that progress will require us to resurrect a pan-periodic chart view of mantle-derived liquids (e.g., Stracke 2012; White 2015), and direct comparisons (e.g., MORB-

normalized, rather than the less-useful but habitual chondrite normalized trace element diagrams) of mantle sources, the latter of which are sorely lacking. Ultimately, we plan to show the efficacy of using combined rock composition, experimental and phase chemical data to better constrain mantle plume sources.

BACKGROUND

Approach & Motivation

Our new trace element analyses of high forsterite (Fo; Mg_2SiO_4) olivine phenocrysts (ca. Fo>85) derive from (1) our archetype of a mantle plume, Hawaii, (2) two continental flood basalt provinces, Deccan and Emeishan, (3) a flood basalt province at a rifted margin, Baffin Island, and (4) a "D-MORB" or "depleted MORB" (derived from an especially chemically depleted DMM, see Waters et al. 2011) from the Siqueiros Transform (Perfit et al. 1996; Putirka et al. 2011), which is part of the East Pacific Rise. We also present new data for olivine grains from Kilbourne Hole mantle xenoliths (often known as "KLB"), collected by the lead author, which we use as both an analytical and petrologic reference.

Our choice of samples is predicated on the idea that oceanic islands and flood basalts are created by thermal mantle plumes, that these plumes have excess heat (Herzberg 1995; Herzberg and Gazel 2009; Li et al. 2012; Putirka 2016), and that they gain much of this heat from the underlying core (e.g., Hess, 1962; Morgan 1971; Lay et al. 2008), or from U-, K- and Th- enriched regions of the lowermost mantle (Garnero et al. 2016). Flood basalts and OIB thus may entrain deep-seated mantle material (e.g., Kellogg et al.

1999; Campbell and O'Neill 2012; Li et al. 2014). In contrast, mid-ocean ridge basalts (MORB) derive from passive upwelling of shallow upper mantle (McKenzie 1967).

A key motivating work is that of Sobolev et al. (2007), who observe that olivine grains from many plumes exhibit peculiarly high Ni contents; they suggest that high Ni-in-Ol requires parental liquids that formed by partial melting of a pyroxenite (rather than peridotite) source. Their pyroxenite source is putatively created by mixing ambient mantle peridotite with partial melts of deeply subducted crust; this reaction may convert a former peridotite source to a near olivine-free, pyroxene-rich lithology. Some dispute this interpretation (e.g., Matzen et al. 2009, 2013; Putirka et al 2011), arguing that high Ni-in-Ol can be obtained by crystallization of mafic magmas over temperatures ranging from 1500^{o}C for moderate Ni contents to 1375^{o}C for the highest Ni-in-Ol (Putirka et al. 2011, their Fig. 5). Others suggest that high Ni-in-Ol reflects mass exchange between a mantle source and Earth's Ni-rich core (Herzberg et al. 2013, but see also Herzberg et al. 2016 for a moderating view). Modeling efforts suggest that pyroxenite- and peridotite-derived partial melts may have similar major oxide compositions (Jennings et al. 2016; Lambart et al. 2016), and our tests indicate the same, although some pyroxenite-derived melts (e.g., Kogiso et al. 2001) range to very low Al_2O_3 (<12 wt. %, with SiO_2/Al_2O_3 ratios >4) and very high CaO (>13.8 wt. %), that are less than typical for peridotite partial melts (mostly >12% Al_2O_3, <14% CaO, $SiO_2/Al_2O_3 < 5$). And surely, Ol compositions derived from such liquids should inherit these characteristics. In addition, trace elements that feature significant contrasts in partitioning behavior between Ol and either of pyroxene or garnet should provide reliable tests. For example, a pyroxenite source should yield Sc-depleted liquids compared to a peridotite source, and Ol grains should inherit such a

mineralogy-dependent influence. In a similar manner, if high Ni contents derive from a core-contaminated mantle, then other (easily analyzed) siderophile elements, such as Co, Cr, Zn and P should also be enriched.

Essential Contrasts Between OIB and MORB: The Influences of Pressures and Temperatures on Partial Melting

A long-observed truth (e.g., Langmuir and Hanson 1980) is that primitive OIB have higher FeO compared to MORB (Fig. 1A). This fact has necessary consequences.

1) Higher FeO in OIB almost certainly results from higher *P*-*T* conditions of partial melting. It is experimentally well-verified that as *P* increases, peridotite partial melts shift towards olivine in composition (Stolper 1980; Longhi 2002) and so *liquids generated at higher* P-T *conditions are enriched in elements compatible in olivine*, such as FeO and MgO (see Langmuir and Hanson 1980), as well as Co and Ni, regardless of source composition. If MORB and OIB are generated from peridotites then major oxide compositions imply OIB genesis at *P* = 20-50 kbar (Fig. 1; Putirka et al. 2011), while MORB are generated at 8-15 kbar (Fig. 1). The necessary effect is that primitive OIBs—and their Ol phenocrysts—have higher Co, Fe and Ni contents relative to MORB as a consequence of partial melting of an olivine-bearing source.

2) Because FeO and other compatible elements are affected by the *P*-*T* conditions of partial melting, seemingly anomalous ratios of Zn/Fe, Mn/Fe, Co/Fe etc., are as likely to reflect mantle melting conditions (e.g., low Zn/Fe = high melt fractions at high *P*-*T* conditions, since these yield high FeO^{liq}) and not necessarily source composition or mineralogy. Our review of peridotite partial melting experiments show that FeO/MnO

ratios are far from constant during partial melting, ranging from 45-60 at P = 40 to 70 kbar, and up to >85 at P = 20 to 35 kbar P (Fig. 1C), and new experiments by Matzen et al. (2017) yield the same result. Undoubtedly, FeO/MnO, and other such ratios also vary with source mineralogy (e.g., Humayun et al. 2004; Le Roux et al. 2010; Davis et al. 2013)—but only variance outside the ranges illustrated in Fig. 1C can disallow a peridotite source, and such variances are insufficiently explored—particularly for a pyroxenite source.

3) It is a grave error to assign an equal T or fractionation extent to olivine grains at an equivalent Fo content. Since OIB have greater FeO than MORB, their Ol grains can only reach an equivalent Fo (as Ol from MORB) when parent magmas have higher MgO, and consequently higher T. The comparison of equivalent Fo contents is tempting, given our familiarity with simple systems (e.g., Bowen and Schairer 1935). But Green et al. (1999) incorrectly hypothesized that MORB and OIB derive from partial melting at equivalent T as both yield Fo91 olivine; their interpretation is flawed because Hawaiian magmas have greater FeO (FeO^{liq}) than MORB (Putirka 2005). For example, if we apply an Fe-Mg exchange coefficient, $K_D(Fe\text{-}Mg)^{ol\text{-}liq}$, of 0.30 (where $K_D(Fe\text{-}Mg)^{ol\text{-}liq} = [X_{FeO}^{ol}/X_{MgO}^{ol}]/[X_{FeO}^{liq}/X_{MgO}^{liq}]$, and X_i^j are mole fractions of i in the phase j), then to crystallize Fo91 olivine from a liquid with 8 wt. % FeO^{liq} (typical of MORB) we must have 13.6% MgO^{liq}. But a liquid with 11 wt. % FeO (typical at Hawaii) must have 18.7% MgO^{liq} to crystallize the very same olivine. Liquids with 13.6 and 18.7% MgO can be produced from the same mantle, but only at very different P-T conditions and melt fractions (F), and the parent liquids (and their equilibrium Ol) will thus have very different trace element contents (Fig. 1).

These and other errors befall any analysis of olivine-compatible elements, as the *P-T* conditions of partial melting are likely to exert a primary control.

Methods

We analyzed major oxides as well as trace elements in olivine that range from lithophile (Ca, Ti, Al, Na, Cu, Sc) to moderately siderophile (Mn, V, Cr, Zn, Co, Ni, P) (see Electronic Appendix 1). Olivine compositions were measured by LA-ICP-MS at the State Key Laboratory of Ore Deposit Geochemistry, Institute of Geochemistry, Guiyang, China; see Liu et al. (2008) for details of methods. In Fig. 2, elements are arranged in order of increasing Ol/(silicate)liq compatibility and metal/silicate compatibility, using Laubier et al. (2014), Le Roux et a. (2015), Siebert et al. (2011; their Table 6) and the GERM website (https://earthref.org/GERM/).

To understand the origin of our Ol compositions we consider how Ol saturated liquids may have evolved, by calculating Liquid and Crystal Lines of Descent (LLDs and CLDs respectively), which trace the evolution of co-existing liquid and crystal compositions (our high Fo Ol grains are from mafic lavas that are Ol saturated only). These curves are derived from olivine/liquid elemental partition coefficients. For the partitioning of Ni between olivine and liquid we use Matzen et al. (2013), supplemented by Jurewicz et al. (1993) and Taura et al. (1998); the latter two studies are mutually consistent with the high-precision work of Matzen et al. (2013) and allow calibration of $D_{\mathrm{Ni}}^{\text{ol-liq}} = f(T)$ to be extended to both higher and lower temperatures (note that Herzberg et al. (2016) provide a precise model $D_{\mathrm{Ni}}^{\text{ol-liq}} = f(D_{\mathrm{MgO}}^{\text{Ol-liq}})$, but our key objective is to make the T-sensitivity of D_{Ni} explicit). Using Jurewicz et al. (1993) only, we obtain:

$$D_{Ni}^{ol\text{-}liq} = e^{\left(\frac{8414}{T} - 4.9\right)} \quad (1a)$$

Equation (1a) is calibrated over the range T = 1140-1325°C at P = 0.0001 GPa, and MgO = 5-10 wt. %. It reproduces the calibration data (n=17) with a standard error of estimate of ±1.3, with R^2 of 0.82. Using Matzen et al. (2013) (0.0001-3 GPa; 1400-1600°C), we obtain:

$$D_{Ni}^{ol\text{-}liq} = e^{\left(\frac{3349}{T} - 0.79\right)} \quad (1b)$$

Combining the Matzen et al. (2013) and Jurewicz et al. (1993) we have:

$$D_{Ni}^{ol\text{-}liq} = e^{\left(\frac{4639}{T} - 1.71\right)} \quad (1c)$$

which reproduces the calibration data (n=29) to ±1.2 with R^2 = 0.85. And combining Matzen et al. (2013), Jurewicz et al. (1993) and Taura et al. (1998) data (3.0-14.4 GPa; 1600-2000°C) yields:

$$D_{Ni}^{ol\text{-}liq} = e^{\left(\frac{5853}{T} - 2.7\right)} \quad (1d)$$

and reproduces the calibration data (n=40) to ±1.0 with R^2 = 0.92. Equation 1d is valid over the ranges T = 1140-2000°C, P = 1 atm – 14.4 GPa, and MgO^{liq} = 5.1-37.5 wt. %.

We also created models using Wang and Gaetani (2008; 0.0001 GPa; 1200-1325°C), whose eclogite liquid-equilibrated olivines yield very high $D_{Ni}^{Ol\text{-}liq}$ ($D_{Ni}^{Ol\text{-}liq}$ = 22), as do some other experiments cited by Le Roux et al. (2015). But as we show below, D_{Ni} from Jurewicz et al. (1993) (Eqn. 1a) appear to better explain certain of our observed plume Ni v. Fo trends.

Because D_{Ni} is sensitive to T, it is possible to use D_{Ni} to estimate T, which for statistical reasons requires a separate calibration. Using Matzen et al. (2013) and Jurewicz et al. (1993) we obtain:

$$T(^oC) = (4.21\times10^{-4} + 1.87\times10^{-4}[ln(D_{Ni})])^{-1} \quad (2)$$

which reproduces T for the calibration data to ±58°C with $R^2 = 0.86$.

To facilitate the calculations of LLD and CLD curves, we also employ two additional empirical equations. First, from stoichiometric and mass balance constraints, we have:

$$Fo^{ol} = 23.55 + 1.3462 MgO^{ol} \quad (3)$$

which reproduces Fo of olivine to ±0.05, with $R^2 = 1.0$. And to predict MgO in Ol we use:

$$MgO^{Ol} = a - \frac{b}{MgO^{liq}} \quad (4)$$

where a = 55.45 and b = 106.1, when $FeOt^{liq}$ (of the equilibrated liquid) is 11.5 wt. %. Equation (4) is specific to $FeOt^{liq}$ content and reproduces MgO^{Ol} to ± 0.1 wt. % with R^2 = 1.0. For $FeOt^{liq}$ = 8% (e.g., MORB), a = 55.63; b = 75.78; for $FeOt^{liq}$ = 13% (high FeO OIB), a = 55.45; b = 120.0).

We also construct LLD and CLD curves for several of the other trace and minor elements in Ol (Ca, Ti, Al, Na, Cu, Sc, Mn, V, Cr, Zr, Co and P); these also make use of Eqns. (3) and (4), and olivine/melt partition coefficients from Laubier et al. (2014), Le Roux et a. (2015) and the GERM website (https://earthref.org/GERM/). While some of these elements quite likely have partition coefficients that are sensitive to T, only the partition coefficients for Mn, Ti and Cr are known with sufficient experimental precision to calibrate $D_i^{ol\text{-}liq} = f(T)$, and so for all other elements we use D_i=constant.

Finally, we calculate mantle source compositions, and test whether such mantle sources were contaminated by a metallic core component. To calculate a mantle source, we use the approach of Putirka (2016) by using observed whole rock compositions (see Fig. 3, caption) as input, to predict an equilibrium Ol composition, and then test whether any such liquids can yield our observed maximum Fo contents observed at each volcanic

system (we assume fO_2 = Ni-NiO; see Putirka 2016). Output from the Putirka (2016) models yields the degree of partial melting, F, and the P-T conditions at which such melt is generated, and an MgO^{liq} for a mantle-equilibrated parental magma. The estimate of F is one of the least certain and yet most important variables when calculating a mantle source, and so we consider a range of predicted values of F in such calculations (see electronic supplements). We then infer the trace element contents of such a liquid from whole rock variation diagrams (see Fig. 3, caption for data). As an example, the concentration of Ni in a parental liquid, Ni^{liq}, is the median concentration of Ni in whole rocks having the calculated values of MgO^{liq}. Table 1 contains a summary of P-T and melt fraction estimates, and the predicted Fo contents of Ol (using Putirka 2016) for our calculated parental magma compositions (additional outputs are in electronic supplement 2). Finally, we use these trace element contents, our predicted T of melting (to estimate D_i when $D_i = f(T)$), our range of predicted values of F, and D_i values from Putirka et al. (2011), updated with partition coefficients from Davis et al. (2013), Laubier et al. (2014), and Le Roux et a. (2015), to calculate a mantle source composition. Putirka et al. (2011) assume batch melting for this calculation, as the error associated with choice of melt model is deemed trivial compared to the errors on estimating a parental magma composition (e.g., Langmuir et al. 1992; Putirka et al. 2011).

Results

Table 1 summarizes our estimates for the P-T conditions of parental magma extraction from the mantle, the melt fraction at extraction, and mantle potential temperatures (T_p)

[assuming fO_2 is buffered at NNO; Putirka 2016)]. Melt fractions are slightly higher than in Putirka et al. (2011), as they are based on new models in Putirka (2016); T_p estimates are slightly lower than in Putirka (2008) because a careful look at just the high precision data of Putirka et al. (2011) indicates slightly lower maximum Fo contents for Ol phenocrysts (at Hawaii, Fo90.5 instead of Fo91.3 in Putirka et al.'s (2011) Table 3 and appendices), and these lower values are consistent with our new results (Fo90.0 for Hawaii; Table 1; electronic appendix 1).

Figure 2 provides a graphical summary of our trace element results. Here, our trace element analyses of Ol grains are compared at a constant value of Fo89 (the highest Fo content common to all our analysis suites), with each plume locality normalized to the trace element contents of Fo89 Ol from our MORB sample (Siqueiros transform). To create Fig. 2, we find the trace element content of Fo89 Ol by taking the average of observed olivine compositions that fall (mostly) in the range Fo87-Fo90 (weighted to yield a mean of Fo89), or for Deccan (where all our Ol compositions are <Fo89), by projecting M v. Fo (where M = a metal cation, such as Co, Na, Ti, etc.) trends back to Fo89, as Klein and Langmuir (1987) correct MORB compositions.

As we discuss below, these trace elements in olivine are controlled by both parent liquid compositions (in turn affected by *P*-*T* conditions of partial melting), and the *P*-*T* conditions of Ol crystallization, and can be divided along lines of partitioning behavior: 1) Elements highly incompatible in olivine ($D_i^{ol\text{-}liq}<<1$). For these (e.g., Ca, Ti, V, Al, Na, Sc), concentrations in Ol tend to be uncorrelated with Fo contents, perhaps because of post-crystallization diffusion for at least some fast-diffusing elements (e.g., Thomson and Maclennan 2013), and because of this, they might not always reliably track liquid

compositions, or source composition. To give an example of the problem, consider that Prytulak and Elliott (2007) observe that plume lavas have elevated Ti relative to MORB—and our plume-derived Ol (except Baffin) are similarly enriched in Ti (Fig. 3A, B); so far, so good. Published experimental values of $D_{Ti}^{ol\text{-}liq}$ range widely (0.003 to 0.21), and we find that only a very low and constant $D_{Ti}^{ol\text{-}liq}$ (=0.007 in Fig. 3A, B) simultaneously yields a Liquid line of Descent (LLD) that reproduces whole rock MgO-TiO_2 trends (Fig. 3A) and a Crystal Line of Descent (or CLD, which tracks crystal compositions with fractionation; see Putirka et al. 2011) that approximates the mean Ti in olivine (but is otherwise insensitive to Fo content; Fig. 3B). So here, we capture the broader inter-suite Ti contents (Fig. 3A), but not at all the intra-suite variations of Ti-in-Ol (Fig. 3B), which suggests that Ti-in-Ol is not controlled by fractionation. And for Sc, we find that at Deccan, and especially Emeishan, Sc-in-Ol is quite high compared to Baffin or Hawaii, despite equivalent or lower Sc in corresponding whole rocks (Fig. 3C, D). This may require a greater $D_{Sc}^{ol\text{-}liq}$ for our continental flood basalt samples, but may reflect non-equilibrium processes (e.g., Shea et al. 2015a, b) or sub-solidus equilibration of Sc-in-Ol with Sc-rich pyroxenitic cumulates. In either case, contrasts in Sc-in-Ol do not directly translate to equivalent contrasts in co-existing liquids, let alone corresponding mantle sources.

2) Elements compatible in Ol ($D_i^{ol\text{-}liq} \geq 1$). Concentrations of some of these elements can closely track liquid compositions (e.g., Ni, Cr). Others (e.g., Mn, Zn) can change dramatically in Ol, even at high Fo contents, even as co-existing liquid compositions change little (Fig. 4A, B)—largely because the concentrations of elements like Mn and Zn in Ol are strongly controlled by temperature. For example, $D_{Mn}^{ol\text{-}liq}$ and $D_{Zn}^{ol\text{-}liq}$ are

close to unity (respectively ranging from 0.8–1.2 and 0.9–1.2; Davis et al. 2013), becoming more compatible at lower *T*. This change towards increasing compatibility is readily evident as Ol crystals become more Mn- and Zn-rich with decreasing Fo (Fig. 4), despite parent liquids having nearly identical and unchanging Mn and Zn contents at high MgO; Figure 4 shows a calculated Ol-only LLD, demonstrating that during fractional crystallization, the evolving, *T*-sensitive, $D_{Mn}^{ol\text{-}liq}$ and $D_{Zn}^{ol\text{-}liq}$ more greatly affect Ol than coexisting liquids. Manganese is an interesting case as parental liquids at Baffin, Hawaii and Emeishan have indistinguishable MnO contents at high MgO, but Ol grains from all three plume localities yield distinct Mn-Fo arrays (Fig. 4B). Examining Ol compositions alone, one could deduce a contrast in mantle source composition, but the whole rock data belie such an interpretation; contrasts in Mn-in-Ol more likely reflect subtle contrasts in crystallization environments. For instance, both the enriched (Emeishan) and depleted (Hawaiian) Mn-in-Ol trends (Fig. 4B) can be produced from a liquid with 1317 ppm Mn (or MnO = 0.17 wt. %), but applying a lower-*T* (1050-1280°C) model of $D_{Mn}^{ol\text{-}liq} = -3.6 + 4500/T(^{o}C)$ for the enriched trend, and a higher-*T* (1150-1400°C) model of $D_{Mn}^{ol\text{-}liq} = -6.2 + 7800/T(^{o}C)$ for the depleted trend (higher *T* yielding lower $D_{Mn}^{ol\text{-}liq}$). Other elements change in more complex ways. Chromium, for example (Fig. 4E, F), is similarly compatible as Mn and Zn ($D_{Cr}^{ol\text{-}liq} = 0.8$; Le Roux et al. 2015), but Cr-in-Ol decreases with decreasing Fo, following parallel changes in liquid MgO-Cr values. Here, Cr contents respond to a rapidly changing liquid composition. These liquids are likely controlled by spinel, and so Cr^{liq} is modeled empirically from whole rock compositions and then Cr-in-Ol is predicted from $D_{Cr} = f(T)$, and $T = f(MgO^{liq})$, using: $Cr^{liq}(ppm) = -118.1 + 56[MgO\ wt.\ \%]$, and $\ln[D_{Cr}^{ol\text{-}liq}] = -2.51 + 3003.3/T(^{o}C)$, which describes the

mean of plume values with an error of ±0.31. Uncertainty on $D_{Cr}^{ol\text{-}liq}$ ($D_{Cr}^{ol\text{-}liq}$ varies from 1.3 to 2.2 at 1500-1525°C; Longhi 2002 and Salters and Longhi 1999) is alone sufficient to encompass all observed Cr-in-Ol values.

Discussion

Ni, Mn and Fe: Measures of Partial Melting Conditions, not Source Composition

The origin of high Ni in olivine from plume lavas has been accredited to a mantle pyroxenite mineralogy (Sobolev et al. 2007), a core-contaminated source at the base of the mantle (Herzberg et al. 2013), or Ni-enriched melts derived by pyroxene fractionation in the crust (Putirka et al. 2011). Our new data support none of these.

To the extent that compatible elements in high Fo olivine might act as a proxy for a mantle source, the predicted patterns of enrichment (or depletion, since the core could just as well absorb siderophile elements from the base of the mantle) deriving from core-mantle equilibration are absent. Cobalt and Zn are nearly as siderophile as Ni (Siebert et al. 2011), but neither are enriched relative to MORB. Perhaps Co and Zn are depleted due to the existence of sulfide phases in evolved lavas, but Cu is enriched (Fig. 2) in our mafic samples, and high *T* near-primary plume magmas are in any case not expected to be sulfide saturated. Meanwhile, mildly siderophile V and Mn, and highly siderophile P (Siebert et al. 2011), are depleted relative to MORB (Fig. 2). We suggest that Ni in plume-derived olivines reflects the high *P*-*T* conditions of plume genesis, and Ol crystallization conditions, as can be discerned from Figs. 5A, B. The key observation is that OIB and MORB fall on the same Ni v. MgO trend (Fig. 5A,B), and so at a given MgO content, OIB and MORB have the same Ni contents. The Baffin plume seems to be

374 slightly depleted in Ni compared to Emeishan and Hawaii at >18% MgO, but the contrast
375 is deceptive: at high MgO (>22 wt. %), whole rock Ni-MgO trends appear to be
376 especially influenced by mixing, between high MgO magmas and olivine grains (Fig 5B),
377 and so contrasts in whole rock Ni contents at high MgO are not necessarily reflective of
378 contrasting mantle sources.

379 Can Any Whole Rocks be Proxies for Liquids?

380 The case for magma mixing at Hawaii, our type example of a mafic volcanic system,
381 is long standing (e.g., Wright and Fiske 1971; Maaloe 1979; Rhodes and Vollinger 2004),
382 but it does not obviate the need for considerable crystallization differentiation. And we
383 can be near certain that liquids exist at nearly all points along the whole rock trend at
384 MgO< 22%. The reason is that Ol compositions occur as a continuum, from Fo71.7 to
385 Fo90.5 (Fig. 5C), requiring a corresponding continuum of liquids with 6.3%-20.8%
386 MgO (Fig. 5D); to deny such is to argue that some fraction of observed Ol phenocrysts
387 have no relationship to Hawaiian magmatism. But then where along the continuum of
388 Fig. 5C does one draw a line to say that "these Ol compositions are irrelevant to
389 Hawaiian magma genesis"?

390 This is not to say, however, that mixing is irrelevant. A range of Hawaiian Ol
391 compositions can be generated by liquids that occupy any part of the gray shaded field in
392 Fig 5D. But because most whole rocks are themselves mostly "liquid" (generally having
393 <30% phenocrysts), it would be nearly impossible to create the observed whole rock
394 trend if the liquids were quite different. And indeed, Hawaiian glass compositions
395 overlap the whole rock trend, to at least 15% MgO (Fig. 5D). So why is the whole rock
396 trend so linear? A large part of the reason is that Ol-only LLDs are quite linear (e.g., Figs.

397 3-5). And so mixing need do little work to straighten out what begin as rather straight
398 trends.

399 Rhodes and Vollinger (2004) further, and in our view correctly, recognize that mixing
400 is not restricted to two end-member compositions, such as one Ol composition, and a
401 single, low-MgO magma. Maaloe (1979) also appreciated this complexity, and
402 emphasized that Hawaiian whole rock trends do not intercept Ol compositional trends at
403 a consistent Fo content. For example, the Rhodes and Volinger (2004) whole rock
404 compositions project to Fo82 for MgO versus Ni, Fo83.7 for MgO versus MnO, and
405 Fo87.2 for MgO versus FeO (using Putirka et al. 2011 Ol compositions). This
406 inconsistency is also visible at the thin-section scale: individual samples (Putirka et al.
407 2011) contain Ol phenocrysts with median and mean Fo contents ranging from at least
408 Fo81 to Fo89. The mixing vectors that produce any one particular sample are thus not
409 necessarily the same as the mixing vectors that produce a compositionally adjacent
410 sample.

411 Rhodes and Vollinger's (2004) solution is to posit that evolved magmas (7% MgO)
412 mix with a range of magmas, having up to 40% MgO (Ol slurries), with liquids ranging
413 to 15% MgO. We would only add that liquids probably range to 21% MgO (to explain
414 high Fo olivine grains), and that the evolved end-member need not be fixed (so in our
415 view, anything can mix with anything). Nonetheless, Fo86 Ol grains are the most
416 common in our new dataset (Fig. 5C). These can be obtained from a liquid with 13.3%
417 MgO, which also is near the mean and median of Hawaiian whole rocks (Fig. 5D). Dry
418 Hawaiian liquids of this composition have densities of 2.8-2.9 g/cm^3 (a little higher if
419 they carry crystals) and so are just the right density to be neutrally buoyant in Hawaii's

middle crust, where thermobarometers place the majority of Hawaiian magma partial crystallization (Putirka 2017, their Fig. 1B). Olivines of Fo86 may be the most common because their equilibrium liquids are the most likely to be trapped in the middle crust. In any case, whole rocks appear to serve as accurate proxies for liquid compositions, up to some upper limit of MgO content, which falls near 21-22% at Hawaii, and which can be determined for any system based on whole rock FeOt values and maximum Fo contents of phenocrysts (see supplementary files for values inferred for the systems studied here and Putirka 2005 for the approach).

Plume-derived olivine grains, then, range to higher Ni compared to MORB because they crystallize from liquids (electronic appendix 2) that are generated at higher *F*, due to higher temperatures of partial melting. Their mantle sources have similar Ni (electronic appendix 3) but higher *F* at plumes leads to greater Ni in the liquids (and their co-existing Ol) that are generated (Table 1). To illustrate, consider a liquid that falls on the Ni-MgO trend, having 20% MgO and 1050 ppm Ni (Fig. 6B); this point forms the "starting point" to the solid gray and black curves in Fig. 6B. To construct the CLDs (gray and black curves) in Fig. 6A and the LLDs (gray and black curves) in Fig. 6B, we use that starting composition and evaluate Eqns. (1a; gray curve) and (1b; black curve) by (i) calculating *T* using the Helz and Thornber MgO-based thermometer (1987; 1416^{o}C at 20% MgO); (ii) we then remove olivine in 2% increments, re-calculating *T*, and (iii) at each step, re-evaluating Eqns. (1a-b) to obtain Ni^{liq}, and using Eqns. (3) and (4), and mass balance to obtain MgO^{liq}, MgO^{Ol} and Fo contents of Ol. Equation (1b) yields Ol with up to 4100 ppm Ni at Fo91, a CLD that reproduces the high-Fo portion of the Hawaiian array (Fig. 6A; black curve), and a LLD that nicely matches Hawaiian whole rocks (Fig. 6B; black

443 curve). Using Eqn. (1a), and the very same starting liquid, we obtain a flatter CLD that
444 reproduces the Ni v. Fo trends at Hawaii, Deccan and Baffin (Fig. 6A; gray curves), and
445 an LLD that reproduces some high Ni vs. MgO whole rock compositions at Hawaii (Fig.
446 6B; gray curves). Equation (1b) also yields a CLD and LLD that nicely reproduces
447 MORB-derived high Fo crystals and whole rock compositions (Figs. 6A, B; blue curve),
448 in this case using a starting liquid with 14.4% MgO^{liq}, Ni^{liq} = 500 ppm, and T = 1301°C.
449 This begs the question of why MORB-derived magmas have lower Ni in the first place,
450 and as we will show, it is because their parental magmas are produced at lower P-T
451 conditions, at lower melt fractions, compared to OIB (Matzen et al. 2009; Putirka et al.
452 2011).

453 These data suggest that not only is the pyroxenite model unnecessary, it is untenable:
454 Ni-enriched sources yield Ni-enriched liquids, which are unobserved (Fig. 6B), and a
455 pyroxenite source predicts Cr-in-Ol that is >>2000 ppm, when Ni contents approach
456 observed values (Fig. 6D). To take the Ni-enrichment case, we show a CLD derived
457 using a parental liquid with 1500 ppm Ni at 20% MgO (from a pyroxenite, or Ni-enriched
458 peridotite, it does not matter); this explains high Ni-in-Ol at Fo≤Fo88 deceptively well
459 (red dashed CLD, Fig. 6A). But the suite of liquids implied by such a CLD have higher-
460 than-observed Ni^{liq} compared to any known whole rock at any MgO (Fig. 6B) when we
461 apply Eqn. 1b and the Helz and Thornber (1987) MgO^{liq} thermometer. Other
462 combinations of thermometers and D_{Ni} models fare no better (Figure 6C). Use of Eqn. 1c
463 does not change the results perceptibly, and if we apply the MgO^{liq} thermometer of
464 Putirka (2008; Eqn. 13), Ni^{liq} contents are further above observed values. If we instead
465 apply Eqn. 1a and the Helz and Thornber (1987) thermometer we can use a parental

magma with just 1200 ppm Ni^{liq} (at 20% MgO) to predict Ni-in-Ol at Fo88, but this curve is still displaced to high Ni^{liq} (Fig 6C), and is worse still if the Putirka (2008) thermometer is applied, and does not even explain Ni-in-Ol patterns. The Cpx-dominated LLD of Putirka et al. (2011) fails more dramatically, for similar reasons, as it predicts liquids with remarkably high Ni contents at lower MgO (Figs. 6A, B, green dashed curves).

Perhaps an even more compelling reason to reject pyroxenite as a source is that Cr and Ni in olivine are very poorly predicted by such. To illustrate, we compare natural Cr and Ni in Ol crystals, to those that would precipitate from a pyroxenite, here using mineral-liquid partition coefficients of Le Roux et al. (2015) and each of the wide ranging pyroxenite mineralogies and melt fractions of Table S3 in Sobolev et al. (2007) (where partial melting ranges from 8 to 79%), as well as their bulk pyroxenite Cr and Ni contents for pyroxenite (e.g., 1710 and 1000 ppm respectively). The predicted Cr-in-Ol contents that would precipitate from pyroxenite-derived liquids are nearly 6 times greater than observed, and plot well off scale in Fig. 6D. If we instead assume that pyroxenites are subducted MORB, and so use the much lower bulk Cr and Ni contents for such (Cr = 296.1 ppm, Ni = 152 ppm; see Putirka et al. 2011), the liquids generated have much lower Cr, as do the equilibrated Ol, but Ni contents are too low (Fig. 6D). In contrast, Ol that precipitates from partial melts of a peridotite work quite well: using a mean bulk peridotite composition having Cr = 2617 ppm and Ni = 2198 ppm (Putirka et al. 2011), and allowing melt fraction to range as $F = 0$ to 0.3, yields Ol crystals that precisely match observed values (Fig. 6D).

Another issue involves the very high Ni-in-olivine at Hawaii at ≤ Fo88, where Ni contents are even higher than at Deccan (Fig. 6A). This might be a signal of Ni-enriched magmas, but the crystal compositions can also be derived from fractionated, FeO-enriched magmas instead (at MgO ≤8 wt. % MgO; Fig. 1A), as shown by the orange curves in Figs. 7A, B. These orange curves connect these high Ni-in-Ol crystals (at ≤Fo88) to a corresponding whole rock MgO^{liq}-Ni^{liq} composition that can serve as a viable equilibrated liquid, at least in the case of Fe-Mg exchange equilibrium. The solutions are not unique, and depend upon the Fe/Mg ratio of the liquid. For this model we use observed Fo in Ol and FeO^{liq} to determine an equilibrium MgO^{liq} (see caption to Fig. 7). And then from the whole rock MgO^{liq}-Ni^{liq} trend (Fig. 7B) we obtain a putative Ni^{liq} value, which we assume is the equilibrium value for $Ni^{Ol} \leftrightarrow Ni^{liq}$ equilibrium. (Fig. 7A) (see caption for equations and details). These results allow us to calculate a putative $D_{Ni}^{ol\text{-}liq}$ for each Ol (Fig. 7A), and to calculate T using Eqn. (2). The temperatures from Eqn. (2) are remarkably close to those obtained from MgO^{liq} using Helz and Thornber (1987) (Fig 7A). An exception involves the lowest Fo Ol in this test (Fo73), where the D_{Ni} value yields a T from Eqn. (2) that is nearly 300°C lower than that obtained from MgO^{liq}. However, the two T estimates are within 20°C if $FeOt^{liq}$ = 18% (Fig. 7B; black connecting line). This is much higher than the FeOt of the host rocks we investigated, but such high values are exhibited by some low-MgO lavas at Hawaii, which may have mixed with our more primitive samples. A test would be to examine high FeOt samples, looking for high Ni Ol grains. In any case, all but the lowest Fo, high Ni-in-Ol crystals have quite little to do with high Ni^{liq}: in diagrams like Figs. 6A or 7A, we can see that it's

not so much that Ni is enriched at a given Fo content, but rather that for a given Ni content, Fo is low.

Peridotite as Plausible Source

Finally, Fig. 7B shows that it is possible to obtain the requisite magmas that can be parental to these high Ni-in-Ol grains by partially melting a peridotite, having 1900 ppm Ni (and 65% Ol, 20% Opx and 15% Cpx), as shown by black and gray curves. These curves show the case for $F = 0.15$, assuming a T of 50°C above the Hirschmann et al. (2002) solidus. To link T and F, we use experimental results from Takahashi et al. (1993), Kushiro (1996) and Pickering-Witter and Johnston (2000), from which we obtain ≈0.18 to 0.31% melt/°C at F <30%. At F > 30%, the results diverge greatly, either maintaining a fertile rate of melt production, or reducing to 0.1% melt/°C; we assume a fertile source (0.3% melt/°C), for reasons discussed below. The Hirschmann et al. (2000) solidus yields array of P-T partial melting conditions, which are then used in Eqn. (1d) to evaluate $D_{Ni} = f(T)$. From partial melting experiments, we also calibrate MgO^{liq} just above the solidus as $MgO^{liq} = -55.96+0.0532[T(^oC)] -2.16[P(GPa)]$, and then also $D_{Ni} = f(MgO^{liq}) = \exp(13.83/MgO^{liq}-0.0147)$. These equations simultaneously yield a Hawaiian primitive magma (MgO^{liq} = 18.8 Wt. %; Ni^{liq} = 815 ppm; Fig. 7B), at P = 3.4 GPa, T = 1521°C. The value of F provides the most important source of error, but at F = 0.2, at 66°C above the solidus we still obtain a magma that falls on the observed whole rock trend (MgO^{liq} = 19.3 Wt. %; Ni^{liq} = 850 ppm; P = 3.5 GPa, T = 1526°C). The results are by no means unique, but they illustrate that peridotites are a plausible mineralogy for plume-source lavas from the localities examined here.

Melting Conditions Assuming a Peridotite Source

As in Putirka (2011), we compare natural whole rock compositions at Hawaii and the EPR to the partial melts generated in experimental studies. Our model parent magmas are combinations of experimentally-derived liquids (see Fig. 1, caption) that, as precisely as possible, fall on a whole rock compositional trend for all of the major oxides, as in Fig. 1. This approach yields conditions of melt extraction of 10 kbar, 1325^{o}C for MORB and 37.5 kbar and 1540^{o}C at Hawaii. The experiments being averaged to achieve a match to observed whole rocks exhibit a 80 to 160^{o}C temperature range for MORB and plumes respectively, and a pressure range of 10-15 kbar for Hawaii; the experimental starting compositions vary as well. We resort to such combinations as no single experiment describes MORB or Plume magmas precisely for every major oxide, while our hypothetical mixtures, provide a very close match. But how then to interpret the *P-T* range? Besides experimental error (e.g., reproducibility, which translated to P-T conditions is about ±30^{o}C and ±1-2 kbar), this almost certainly represents the challenge of searching *P-T*-composition space to find the "just so" conditions to explain natural magmas. But crucially, melting is not an isothermal, isobaric process. Our P-T estimates represent a mean set of conditions over which melt was equilibrated within the mantle, and the starting compositions of the experiments we employ represent an average composition of what we know to be a heterogeneous source. For our Plume 1 model then, the *P-T* ranges exhibited by our averaged experiments (45-30 kbar; 1620-1460^{o}C) might represent very real variations in what is assuredly a polybaric, polythermal partial melting process.

While Emieshan and Deccan have major oxides that are quite similar to Hawaii, Baffin Island is clearly a special case, since except for FeOt and SiO_2, its lavas are otherwise quite similar to our MORB samples—for example Baffin lavas have elevated Al_2O_3 compared to other plumes (Fig. 8C). The Baffin Al_2O_3 contents might seem to contradict our high T_P, since this should also require elevated pressures, and at high-*P* garnet may be present in the solid residue. But high-*P* partial melting experiments exhibit more than sufficient scatter to accommodate Baffin lavas. For example, the 30 kbar model partial melts of Longhi (2002) match Al_2O_3 and other oxides at Baffin quite nicely, as do yet higher *P* experiments by Takahashi et al. (1993; 46 kbar, 1800^{o}C) and Walter (1998; 45 kbar, 1650^{o}C), which both fall on the high-MgO end of the Baffin compositional spectrum. A problem with Al_2O_3, then is that it decreases with increasing MgO. So while experimental data do indeed show decreasing Al_2O_3 in equilibrated melts as *P* increases, there is enough scatter in these to cover both the Baffin and Hawaiian lavas at high MgO. So the key question is whether we must match Al_2O_3 at the high or low MgO end of an observed whole rock trend? The answer is found with FeOt. High pressures are required to explain Baffin's high FeOt compared to MORB (10-11 wt. % at Baffin, compared to 8% for MORB, when MgO>10%). So we find that, like Hawaii, high T_p and melting pressures in the 30-45 kbar range are most consistent with observed Ol and lava compositions.

These *P*-*T* conditions, though, leave unexplained the fact that Baffin and MORB share similar, elevated Al_2O_3 contents relative to Hawaii and other plumes (Fig. 8), as well as lower TiO_2, and slightly elevated CaO, the latter being perhaps also in common with

Deccan. We hypothesize that these contrasts reflect differences in source regions, as indicated by other elements as well (see following discussion of Fig. 9).

Tests of a Pyroxenite Source: Ca, Al and Sc

We might expect that pyroxenite-influenced melts and crystals would be enriched in Ca and Al (or perhaps depleted if a high mode of Cpx during melting overrides the higher bulk concentrations): pyroxenite source materials have 7-22 wt. % Al_2O_3 and 2-14% CaO (Kogiso et al. 1998; Kogiso and Hirschmann 2001; Petermann et al. 2004; Lambart et al. 2009; Tsuno and Dasgupta 2011), while peridotites have lower Al_2O_3 and CaO (3.6-4.3 wt. % and 3.2-3.5 wt. % respectively; Walter 1998). However, peridotite partial melts alone yield a wide range of CaO^{liq} and $Al_2O_3{}^{liq}$. Ocean Island Basalts have lower CaO^{liq} and $Al_2O_3{}^{liq}$ than MORB, and the contrasts are expected given current experimental studies, if the contrasting pressures required by Fe and Mn apply (Fig. 1; see also Putirka et a. 2011), i.e., P = 30-50 kbar for Hawaii and 10 kbar for MORB. Our low-P MORB model (Fig. 1) yields 11.6 wt. % CaO^{liq} and 14% $Al_2O_3{}^{liq}$ at 13.1 wt. % MgO^{liq} (and 8% $FeOt^{liq}$), while our "Plume Model 2" (Fig. 1) has 8% CaO^{liq} and 9% $Al_2O_3{}^{liq}$ at 20.6% MgO^{liq} (and 11.5% $FeOt^{liq}$). It seems clear that Ca and Al are lower in high Fo Hawaiian Ol compared to MORB (Figs. 8B, D) as each reflects their contrasting parent liquids (Fig. 8A).

At Baffin, despite having a much greater mantle potential T_p than MORB (Table 2), these lavas exhibit similar Ca and Al contents to MORB for both whole rocks and olivine. Since the whole rock CaO and Al_2O_3 contents of both MORB and Baffin are explained by peridotite partial melting, at low and high P-T conditions respectively, we

cannot exclude a pyroxenite source, but have no reason to propose one. At Emeishan, however, olivine compositions range to distinctly high Ca despite their whole rocks having no more CaO than other lavas. Might the elevated Ca-in-Ol at Emeishan indicate the kind of garnet-pyroxenite source that Sobolev et al. (2007) suggested for Hawaii? This may be the case, as Emeishan lavas also have greater Sc-in-Ol and greater Sc in their whole rocks compared to Hawaii (Figs. 3C, D). Perhaps partial melting of a Ca- and Sc-rich source, e.g., pyroxene-rich, might be the cause. But there are problems with this model. Emeishan parent liquids are not the most Sc-enriched (Fig. 3C), ranging to 30 ppm Sc at 20% MgO, compared to 35 ppm Sc at Baffin (Fig. 3C), even though Emeishan Ol grains have the highest Sc-in-Ol values (22 ppm on average; Fig. 3D). No experimentally determined values for $D_{Sc}^{ol\text{-}liq}$ can explain these contrasts. For example, $D_{Sc}^{ol\text{-}liq}$ ranges to about 0.25 (Davis et al. 2013; Laubier et al. 2014), and for a liquid with 30 ppm Sc, a $D_{Sc}^{ol\text{-}liq}$ of 0.73 is required to obtain Sc-in-Ol of 22 ppm—nearly three times the highest experimental value (and Laubier et al. see no dependency of $D_{Sc}^{ol\text{-}liq}$ on T or fO_2, so we cannot at the present call on changes in such to increase $D_{Sc}^{ol\text{-}liq}$). Likewise, applying $D_{Sc}^{ol\text{-}liq} = 0.25$ requires a liquid with 89 ppm Sc (more than double observed Emeishan whole rock values; Fig. 3C) to precipitate Ol with 22 ppm Sc. So it would be a tenuous conclusion at best to link Emeishan Sc-in-Ol contents to enriched liquids, let alone enriched source materials. Finally, Lambart et al. (2009) report very low Al-in-Ol for their pyroxenite-equilibrated Ol, well below anything we observe at Emeishan, Deccan, Siqueiros or Hawaii (Fig. 8D). Given these problems for a pyroxenite source, we posit that high Ca-in-Ol at Emeishan might instead reflect lower P-T conditions of crystallization (e.g., Stormer 1973; Koehler and Brey 1988), consistent with higher Mn-

in-Ol at Emeishan (Fig. 4B). But thermobarometry (Tao et al. 2015) at Emeishan indicates high *P-T* equilibration conditions for picrites, so Sc and Ca in Ol might instead reflect non-equilibrium processes (e.g. Shea et al. 2015a, b).

Mantle Source Compositions from Parental Liquids (and maximum Fo in Ol)

Although Ol trace element compositions do not easily translate to a mantle composition, their Fo contents delimit parent liquid compositions, which provide a more direct inference of mantle source. Applying Putirka et al.'s (2011) melting models with Putirka (2016) for melt fraction estimates, we obtain mantle compositions as in Figures 9-10, where elements are arranged in order of decreasing enrichment at Hawaii relative to our calculated Siqueiros-MORB mantle, moving from left to right. To model the MORB source we rely on the very primitive lavas from the East Pacific Rise (Siqueiros Transform; Perfit et al., 1996; Hays, 2004) as they are closer to putative primary magmas, and so minimize error in reconstructing a MORB mantle source.

We find that the mantle source regions of Hawaii, Deccan and Emeishan share similar patterns and magnitudes of enrichments in incompatible elements relative to the MORB source mantle (DMM) (except for lower Cr; Fig. 9). This is not to say that our inferred plume sources are identical; they are not (e.g., Willbold and Stracke 2006), but we affirm prior work that indicates broadly shared enrichments among plumes sources (e.g., Willbold and Stracke, 2006; Arevalo et al. 2013). Our Hawaiian source is also enriched relative to the pyrolite models of McDonough and Sun (1995) and Lyubetskaya and Korenaga (2003) (Fig. 9B). Baffin, despite having plume-like T_p (Table 1), interestingly has a mantle source with trace element contents that are quite similar to that for MORB,

except for being slightly enriched relative to our estimate of Cr (Fig. 9A); however, within uncertainties (see error bars in figures) the Baffin Island plume source overlaps with the sources for the other three plumes examined here. Interestingly, Jackson and Jellinek (2013) find that the Baffin source is slightly less depleted in Large Ion Lithophile Elements (LILE) than DMM than in the model used here. However, they infer lower degrees of partial melting: 14%, instead of 24% in this study (Table 1). Nonetheless, the Baffin Island plume composition considered here is within error of the composition calculated in Jackson and Jellinek (2013) and requires no addition of enriched sources to explain trace element concentrations. We should perhaps emphasize that, due to its very high $^{3}He/^{4}He$, Baffin is not the same as MORB; but the trace element similarities of the Baffin source and DM provides an apparent striking affinity.

In contrast, trace elements are enriched relative to DM (and the Baffin source) at Hawaii, Deccan and Emeishan, and by applyjng methods of Putirka et al. (2011) we invert our calculated melt compositions to estimate source compositions. We find that Hawaiian, Deccan and Emeishan enrichments can be explained by adding 18-24% average ocean crust (MORB) to DMM of Workman and Hart (2004). Our estimate of the amount of crust added back to the non-Baffin plume-source mantle is greater than in Putirka et al. (2011), as that earlier work assumed smaller degrees of partial melting (10%) for the Hawaiian source. Melt fraction estimates are quite uncertain, and so the actual amounts, if the general approach is correct, probably lie somewhere between those earlier values and our current estimates (see electronic appendix 3). What is especially compelling, though, is that nearly identical proportions of MORB and DMM simultaneously explain elements that are chemically quite different. The errors in such

669 mantle estimates are non-trivial (20-140% for compatible to incompatible elements), but
670 within such error our Hawaiian source estimates match our MORB + DMM pyrolite
671 model for all elements. Moreover, calculated MORB:DMM ratios are similar using
672 differently-derived estimates of both MORB and DMM (Fig. 10A).

673 So why then does Baffin lavas range to higher $^{3}He/^{4}He$ than, say, Hawaii? It has long
674 been recognized that high $^{3}He/^{4}He$ at Hawaii is inversely correlated with $^{87}Sr/^{86}Sr$ (Hauri
675 and Kurz 2002), and other studies, e.g., Jackson et al. (2008) and Grapic et al. (2015),
676 propose that the Baffin source is the receiver of subducted materials and the source of
677 high $^{3}He/^{4}He$ in plumes and that subducted oceanic crust provides the enriched TITAN
678 character as proposed by Jackson et al. (2008).

679 Because so many different elements (lithophile, chalcophile and moderately
680 siderophile) at Hawaii, Emeishan and Deccan are explained by a pyrolite-like source, this
681 would seem to argue against a peculiar mineralogy (e.g., pyroxenite) or intra-mantle
682 fractionation (e.g., bridgmanite) to explain plume compositions inferred from the lavas in
683 this study. Zhang et al. (2016) nonetheless intimate that wadsleyite may preferentially
684 partition Ti, V and Cr, while Bindi et al. (2017) report on a Ti-rich form of bridgmanite.
685 To be fair, neither of these studies attempt to explain plume compositions. Perhaps even
686 more interesting is the possibility of an Fe-enriched lower mantle (Kaminsky and Lin,
687 2017). But Fe-enrichments in OIB appear to be not so great as to be produced from a
688 mantle with a major element composition similar to MORB, and we find no pronounced
689 coupled enrichments in Ti and V that accompany Cr. Nor is it clear that the accumulation
690 of Ti-bridgmanite might yield the complete array of enrichments of Fig. 9A. This is not
691 to say that intra-mantle fractionation might not influence plume composition, but it would

be an odd coincidence that such a process was global in nature and would precisely mimic the addition of oceanic crust to a DM source.

Implications

Our Baffin Island results are perhaps the most interesting. The Baffin source is quite hot, and we infer that it is rooted in as deep a part of the mantle as any other mantle plume. But the Baffin source is also depleted, as reflected in both its major oxides and trace elements, in a way that remarkably mimics the MORB source. Plumes other than Baffin, by contrast, require at least 20-25% subducted MORB-crust to be mixed back into a depleted MORB mantle source, to explain their bulk compositions. We appreciate that the Baffin and MORB sources cannot be equivalent: MORBs have low $^{3}He/^{4}He$ (~8 Ra) compared to the Baffin mantle (up to 50 Ra). Additionally, if we accept W isotope results (Rizo et al. 2016), that indicate that the Baffin source has been isolated from the rest of the mantle for 4.5 Ga, then the Baffin source was depleted at that early date. The depletion of the MORB source, by contrast, occurred much later, as it is a residue remaining after a presumably much later and prolonged continental crust extraction event. There are several options to explain the MORB-Baffin contrast: The Baffin source could be 1) perfectly unique—an ancient depleted source at the base of the mantle, with an as yet unknown enriched counterpart, that otherwise matches MORB only by coincidence, 2) a depleted matrix that pervades the lowermost mantle that elsewhere receives subducted crust, but beneath Baffin, has been strangely resistant to such accumulation, 3) related to the MORB source, where the materials that would eventually form the crust were extracted into the upper part of the mantle at or before 4.5 Ga only to

be gradually tapped over the next 4.5 Ga from relatively shallow mantle only, leaving a shallow depleted MORB source, and a deeper Baffin source (again, resistant to subducted crust accumulation), 4) is not from a source that feeds other mantle plumes—representing something deeper still. None of these are terribly satisfying, or mutually exclusive. But Baffin is isotopically close to PREMA (Zindler and Hart 1986; having just slightly lower $^{206}Pb/^{204}Pb$) and FOZO (Hart et al. 1992)—and so if Baffin can be shown to be *uniquely old* among plumes (being presumably *uniquely unaffected* by admixtures of young subducted crust), Baffin may then represent a rare sampling of Earth's most ancient mantle (Jackson et al., 2010).

Some of these results are not entirely new: Herzberg et al. (2007) infer that Baffin is hot, while Starkey et al. (2012) demonstrate that, despite having plume-like high $^{3}He/^{4}He$, Baffin is depleted compared to most plumes. Garnero et al. (2016) suggest that geochemical anomalies among ocean island basalts carry no information about source depth, and with one exception, we concur—that exception being high $^{3}He/^{4}He$, which along with high T_p are the only viable indicators of deep-seated plumes, past or present (Putirka 2008). And we agree with Jackson et al. (2017) that to hide something like the Baffin source for an extended period of time, it must be quite dense, and quite deep. Given that $^{87}Sr/^{86}Sr$ is negatively correlated with $^{3}He/^{4}He$ at Hawaii, and trends toward a Baffin-like composition (see Fig. 1A of Hauri and Kurz 2002), we propose that a Baffin-like source, or perhaps the Baffin source itself, is the wellspring of high $^{3}He/^{4}He$ in plumes, and whose $^{3}He/^{4}He$ values are slightly diluted due to mixing of subducted crust.

Despite the Baffin enigma, we appear to know the depleted MORB source with confidence. Estimates derived from very different mass balances of primitive melt and

738 peridotite samples (Salters and Stracke 2004; Workman and Hart 2005; Putirka et al.
739 2011) yield quite similar results. This should be expected, since residual peridotites and
740 parental magmas are complementary derivatives of a common source and process. But
741 the convergence also confirms that we have, at least roughly, correctly identified parental
742 magmas and the processes and conditions under which they are created.

743 Finally, we confirm the current view of the deep mantle as a "graveyard" of subducted
744 MORB crust (Wyession 1996; White 2015), but we reject the idea that this graveyard is
745 necessarily resurrected with a pyroxenite mineralogy (e.g., Hofmann and White, 1982);
746 we estimate that plumes entrain up to 25% subducted oceanic crust, rather than the nearly
747 100% indicated in the original model (Baffin providing a 0% end-member case). This
748 material seems to be thoroughly admixed, with no clear evidence of a mineralogically
749 distinct signal. Kogiso et al (2004) suggest otherwise, but as we show in an electronic
750 supplement (ES1), their pyroxenite end-member is arbitrary and trace element ratios do
751 not indicate a mineralogically distinct source for elevated $^{187}Os/^{188}Os$.

752 The deep mantle plume source is, however, significantly enriched compared to earlier
753 "pyrolite" models (McDonough and Sun 1995; Lyubetskaya and Korenaga 2010) and
754 may well be what is perceived in seismic studies (e.g., Zhao et al. 2015). Our estimates,
755 perhaps not coincidentally, are also quite close to Ringwood's (1962) basalt:dunite ratio
756 of 1:4. Such high amounts of added crust may create an untenably "hyperfertile" source,
757 with too much garnet to explain certain trace element ratios (Norman and Garcia 1999;
758 Putirka et al. 2011). But our higher MORB:DMM ratios emanate from higher estimates
759 of melt fraction (using Putirka 2016 instead of Putirka et al. 2007), which may allow
760 sufficiently high dissolution of garnet to allay the key objection: Walter's (1998)

761 experiments yield just 10% garnet (of all phases, including liquid) at 20% melting at 6
762 GPa, and no garnet at all at the same degrees of melting at 3 GPa. In any case, Baffin
763 Island shows that this slab graveyard is not ubiquitous (i.e., recycled slabs do not
764 permeate all deep mantle reservoirs), either because subducted slabs are unevenly
765 interred, or they can be efficiently excavated in later plume upwelling events, or perhaps
766 because the Baffin source lies below this graveyard, as a dense under-layer (e.g., Jackson
767 et al. 2017) that for some reason is not tapped at yet hotter flood basalt provinces.
768

769 **Acknowledgements**

770 K. Putirka would like to thank both Eric Brown and Andrew Matzen for extremely
771 thoughtful and detailed reviews that challenged us to think through our assumptions and
772 conclusions. We also thank NSF for support to K. Putirka that indirectly helped support
773 some of this work, in the form of grants NSF-EAR 1250322, 1250323. M. Jackson
774 acknowledges support from NSF-EAR 1624840. Yan Tao would like to thank NSF of
775 China 41473051.
776
777 **References Cited**
778

779 Arevalo, R. Jr., Mcdonough, W.F., Stracke, A., Willbold, M., Ireland, T.J., and Walker,
780 RJ. (2013) Simplified architecture and distribution of radiogenic power.
781 Geochemistry, Geophysics, Geosystems, 14, doi: 10.1002/ggge.20152.
782 Baker, M.B., Hirschmann, M.M., Ghiorso, M.S., Stolper, E.M. (1995) Compositions of
783 near-solidus peridotite melts from experiments and thermodynamic calculations.
784 Nature 375, 308–311.
785 Bender, J.F., Langmuir, C.H., and Hanson, G.N. (1984) Petrogenesis of basalt
786 glasses from the Tamayo Region, East Pacific Rise. Journal of Petrology,
787 25, 213–254.
788 Bindi, L., Sirotkina, E., Bobrov, A.V., Walter, M.J., Pushcharovsky, D., and Irifune, T.
789 (2017) Bridgmanite-like crystal structure of the novel Ti-rich phase synthesized at
790 transition zone condition. American Mineralogist, 102, 227-230.
791 Bouvier, A., and Boyet, M. (2016) Primitive solar system materials and Earth share a
792 common initial ^{142}Nd abundance. Nature, 537, 399-402.
793 Bowen, N.L. and Schairer, J.F. (1935) The system MgO-FeO-SiO2, American Journal of
794 Science, 29, 151-217.
795 Campbell, I.H. and O'Neill, H. St. C. (2012) Evidence against a chondritic Earth. Nature,
796 483, 553-558.
797 Cottrell, E., and Kelley, K.A. (2011) The oxidation state of Fe in MORB glasses and the

oxygen fugacity of the upper mantle. Earth and Planetary Science Letters, 305, 270-282.

Davis, F.A., Humayun, M., Hirschmann, M.M., and Cooper, R.S. (2013) Experimentally determined mineral/melt partitioning of first-row transition elements (FRTE) during partial melting of peridotite at 3 GPa. Geochimica et Cosmochimica Acta, 104, 232-260.

Gale, A., Dalton, C.A., Langmuir, C.H., Su, Y. and Schilling, J-G. (2013) The mean composition of ocean ridge basalts. Geochemistry, Geophysics, Geosystems, 14, doi:10.1029/2012GC004334.

Garapic, G., Mallik, A., Dasgupta, R., and Jackson, M.G. (2015) Oceanic lavas sampling the high $^{3}He/^{4}He$ mantle reservoir: primitive, depleted or enriched? American Mineralogist, 100, 2066-2081.

Garnero, E., McNamara, A.K., Shim, S-H. (2016) Continent-sized anomalous zones with low seismic velocity at the base of Earth's mantle. Nature Geoscience, 9, 481-489.

Green, D. H., T. J. Falloon, S. M. Eggins, and G. M. Yaxley (1999), Primary magmas and mantle temperatures, European Journal of Mineralogy, 13, 437–451.

Grove, T.L. and Bryan, W.B. (1983) Fractionation of pyroxene-phyric MORB at low pressure: an experimental study. Contributions to Mineralogy Petrology, 84, 293-309.

Grove, T.L. and Juster, T.C. (1989) Experimental investigations of low-Ca pyroxene stability and olivine-pyroxene liquid equilibria at 1-atm in natural basaltic and andesitic liquids. Contributions to Mineralogy Petrology, 103, 287-305.

Hauri, E.H., and Kurz, M.D. (2002) Melt migration and mantle chromatography, 2: a time-series Os isotopic study of Mauna Loa volcano, Hawaii. Earth and Planetary Science Letters, 153, 21-36.

Hawkesworth, C.J., Norry, M.J., Roddick, J.C., and Vollmer, R. (1979) $^{143}Nd/^{144}Nd$ and $^{87}Sr/^{86}Sr$ ratios from the Azores and their significance in LIL-element enriched mantle. Nature, 280, 28-31.

Hart, S.R., Hauri, E.H., Oschmann, L.A., and Whitehead, J.A. (1992) Mantle plumes and entrainment: isotopic evidence. Science, 256, 517-520.

Hays, M.R. (2004) Intra-transform volcanism along the Siqueiros Fracture Zone 8°20' N–8°20'N, East Pacific Rise. Ph.D. Thesis, University of Florida, 251 p.

Helz, R.T., and Thornber, C.R. (1987) Geothermometery of Kilauea Iki lava lake, Hawaii. Bulletin of Volcanology, 49, 651-668.

Herzberg, C. (1995) Generation of plume magmas through time: an experimental perspective. Chemical Geology, 126, 1-16.

Herzberg, C., Asimow, P.D., Arndt, N., Niu, Y., Lesher, C.M., Fitton, J.G., Cheadle, M.J., Saunders, A.D. (2007) Temperature in ambient mantle and plumes: constraints from basalts, picrites and komatiites. Geochemistry, Geophysics, Geosystems, 8, doi:10.1029/2006GC001390.

Herzberg, C., Asimow, P., Ionov, D., Vidito, C., Jackson, M.G., and Geist, D. (2013) Nickel and helium evidence for melt above the core-mantle boundary. Nature, 493, 393-397.

Herzberg, C. and Gazel, E. (2009) Petrological evidence for secular cooling in mantle plumes. Nature, 458, 619-623.

Herzberg, C., Vidito, C. and Starkey, N.A. (2016) Nickel-cobalt contents of olivine record origins of mantle peridotite and related rocks. American Mineralogist, 101,

1952-1966.
Herzberg, C., Zhang, J. (1996) Melting experiments on anhydrous peridotite KLB-1; composition of magmas in the upper mantle and transition zone. Journal of Geophysical Research 101, 8271–8295.
Hess, H.H. (1962) History of the ocean basins: In: Engle, A.E., James, H.L., Leonard, B.F. eds., Petrologic Studies: A Volume in Honor of A.F. Buddington. Geological Society of America, 599-620.
Hirschmann, M.M. (2000) Mantle solidus: experimental constraints and the effects of peridotite composition. Geochemistry, Geophysics, Geosystems 1 (2000GC000070).
Hirschmann, M.M., and Stolper, E.M. (1996) A possible role for garnet pyroxenite in the origin of the "garnet signature" in MORB. Contributions to Mineralogy and Petrology, 124, 185-208.
Hofmann, A.W. (1997) Mantle geochemistry: the message from oceanic volcanism. Nature, 385, 219-229.
Hofmann, A.W., and White, W.M. (1982) Mantle plumes from ancient oceanic crust. Earth and Planetary Science Letters, 57, 421-436.
Humayun, M., Qin, L., and Norman, M. (2004) Geochemical evidence for excess iron in the mantle beneath Hawaii. Science, 306, 91-94.
Jackson, M.G. and Carlson, R.W. (2012) Homogeneous superchondritic $^{142}Nd/^{144}Nd$ in the mid-ocean ridge basalt and ocean island basalt mantle. Geochemistry, Geophysics, Geosystems, 13, doi:10.1029/2012GC004114.
Jackson, M.G., Carlson, R.W., Kurz, M.D., Kempton, P.D., Francis, D., and Blusztajn, J. (2010) Evidence for the survival of the oldest terrestrial mantle reservoir. Nature, 466, 853-856.
Jackson, M.G., Hart, S.R., Saul, A.E., Shimizu, N., Jurz, M.D., Blusztjan, J.S., and Skovgaard, A.C. (2008) Globally elevated titanium, tantalum, and niobium (TITAN) in ocean island basalts with high $^{3}He/^{4}He$. Geochemistry, Geophysics, Geosystems, 9, Q04027.
Jackson, M.G., and Jellinek, A.M. (2005) Major and trace element composition of the high $^{3}He/^{4}He$ mantle: implications for the composition of a non-chondritic Earth. Geochemistry, Geophysics, Geosystems, 14, doi:10.1002/ggge.20188.
Jackson, M.G., Konter, J.G., and Becker, T.W. (2017) Primordial helium entrained by the hottest mantle plumes. Nature, 542, 340-344.
Jennings, E.S., Holland, T.J.B., Shorttle, O., Maclennan, J., and Gibson, S.A. (2016) The composition of melts from a heterogeneous mantle and the origin of ferropicrite: application of a thermodynamic model. Journal of Petrology, 57, 2289-2310.
Jurewicz, A.J.G., Mittlefehldt, D.W., and Jones, J.H. (1993) Experimental partial melting of the Allende (CV) and Murchison (CM) chondrites and the origin of asteroidal basalt. Geochimica et Cosmochimica Acta, 57, 2123-2139.
Kaminsky, F.V., and Lin, J-F. (2017) Iron partitioning in natural lower-mantle minerals: toward a chemically heterogeneous lower mantle. American Mineralogist, doi:10.2138/am-2017-5949.
Kellogg, L.H., Hager, B.H., and van der Hilst, R.D. (1999) Compositional stratification in the deep mantle. Science 283, 1881–1884.
Klein, E. M., and C. H. Langmuir (1987), Global correlations of ocean ridge basalt chemistry with axial depth and crustal thickness, Journal of Geophysical Research, 92,

8089–8115.
Kogiso, T., Hirose K., and Takahashi, E. (1998) Melting experiments on homogeneous mixtures of peridotite and basalt: applications to the genesis of ocean island basalts. Earth and Planetary Science Letters, 162, 45-61.
Kogiso, T., and Hirschmann, M.M. (2001) Experimental study of clinopyroxenite partial melting and the origin of ultra-calcic melt inclusions. Contributions to Mineralogy and Petrology, 142, 347-360.
Kogiso, T., Hirschmann, M.M., and Reiners, P.W. (2004) Length scales of mantle heterogeneities and their relationship to ocean island basalt geochemistry. Geochimica et Cosmochimica Acta, 68, 345-360.
Koehler, T., and Brey, G.P. (1988) Ca in olivine as a geobarometer for lherzolites. Chemical Geology, 70, 10.
Kushiro, I. (1996) Partial melting of a fertile mantle peridotite at high pressures: an experimental study using aggregates of diamond. In: Basu, A. & Hart, S., eds., Reading the Isotopic Code. American Geophysical Union, Geophysical Monograph 95, 109-122.
Lambart, S., Baker, M.B., and Stolper, E.M. (2016) The role of pyroxenite in basalt genesis: Melt-PX, a melting parameterization for mantle pyroxenites between 0.9 and 5 GPa. Journal of Geophysical Research, 121, 5708-5735.
Lambart, S, Laporte, D. and Schiano, P. (2009) An experimental study of pyroxenite partial melts at 1 and 1.5 GPa: implications for the major-element composition of mid-ocean ridge basalts. Earth and Planetary Science Letters, 288, 335-347.
Langmuir, C.H. and Hanson, G.N. (1980) An evaluation of major element heterogeneity in the mantle sources of basalts. Philosophical Transactions of the Royal Society of London, A 297, 383-407.
Langmuir, C. H., Klein, E. M. & Plank, T. (1992) Petrological systematics of mid-ocean ridge basalts: constraints on melt generation beneath ocean ridges. In: Morgan, J. P., Blackman, D. K. & Sinton, J. M. (eds) Mantle Flow and Melt Generation at Mid-Ocean Ridges. American Geophysical Union, Geophysical Monograph 71,183-280.
Lassiter, J., and Hauri, E. (1998) Osmium-isotope variations in Hawaiian lavas: evidence for recycled oceanic lithosphere in the Hawaiian plume. Earth and Planetary Letters, 164, 483-496.
Lassiter, J.C., Hauri, E.H., Reiners, P.W., and Garcia, M.O. (2000) Generation of Hawaiian post-erosional lavas by melting of a mixed lherzolite/pyroxenite source. Earth and Planetary Letters, 178, 269-284.
Laubier, M., Grove, T.L., Langmuir, C.H. (2014) Trace element mineral/melt partitioning for basaltic andesitic melts: an experimental and laser ICP-MS study with application to the oxidation state of mantle source regions. Earth and Planetary Science Letters, 392, 265-278.
Lay, T., Hernlund, J., and buffett, B.A. (2008) Core-mantle boundary heat flow. Nature Geoscience, 1, 25-32.
Le Roux, V., Dasgupta, R., and Lee, C-T.A. (2010) First series transition metals (Zn, Fe, Mn, Co, Sc, V) as tracers of mineralogic heterogeneities in the mantle. Geochimica et Cosmochimica Acta, 74, A582.
Le Roux, V., Dasgupta, R., and Lee, C-T.A. (2015) Recommended mineral-melt partition coefficients for FRTEs (Cu), Ga, and Ge during mantle melting. American

936 Mineralogist, 100, 2533-2544.
937 Li, M., McNamara, A.K., and Garnero, E.J. (2014) Chemical complexity of hotspots
938 caused by cycling oceanic crust through mantle reservoirs. Nature Geoscience, 7, doi:
939 10.1038/NGEO02120.
940 Li, C., Tao, Y., Qi, L., and Repley, E.M. (2012) Controls on PGE fractionation in the
941 Emeishan picrites and basalts: Constraints from integrated lithophile-siderophile
942 elements and Sr-Nd isotopes. Geochimica et Cosmochimica Acta, 90, 12–32.
943 Liu Y.S., Hu Z.C., Gao S., Günther D., Xu J., Gao C.G. and Chen H.H. (2008) In situ
944 analysis of major and trace elements of anhydrous minerals by LA-ICP-MS without
945 applying an internal standard. Chemical Geology, 257, 34-43.
946 Longhi, J. (2002). Some phase equilibrium systematics of lherzolite melting: I.
947 Geochemistry, Geophysics, Geosystems, 3, doi: 10.1029/2001GC000204.
948 Lyubetskaya, T. and Korenaga, J. (2007) Chemical composition of Earth's primitive
949 mantle and its variance: 1. Methods and results. Journal of Geophysical Research, 112,
950 doi:10.1029/2005JB004223.
951 Maaløe, S. (1979), Compositional range of primary tholeiitic magmas evaluated from
952 major-element trends, Lithos, 12, 59–72.
953 Matzen, A. K., Baker, M. B., Beckett, J. R. & Stolper, E. M. (2009) The temperature and
954 pressure dependence of Ni partitioning between olivine and MgO-rich silicate melt.
955 Goldschmidt Conference Abstracts A851.
956 Matzen, A.K., Baker, M.B., Beckett, J.R., and Stolper, E. (2013) The temperature and
957 pressure dependence of nickel partitioning between olivine and silicate melt. Journal
958 of Petrology, 54, 2521-2545.
959 Matzen, A.K., Wood, B.J., Baker, M.B., and Stolper, E.M. (2017) The roles of pyroxenite
960 and peridotite in the mantle sources of oceanic basalts. Nature Geoscience, 10, 530-
961 535.
962 McDonough, W.F. and Sun, S-S. (1995) The composition of the Earth. Chemical
963 Geology, 120, 223-253.
964 McKenzie, D. (1967) Some remarks on heat flow and gravity anomalies. Journal of
965 Geophysical Research, 72, 6261-6273.
966 Moore, J.M. and New Horizons Science Team (2016) The geology of Pluto and Charon
967 through the eyes of New Horizons, Science, 351, 1284-1293.
968 Morgan, W.J. (1971) Convection plumes in the lower mantle. Nature 230, 42-43.
969 Norman, M.D., Garcia, M.O. (1999) Primitive magmas and source characteristics of the
970 Hawaiian plume: petrology and geochemistry of shield picrites. Earth and Planetary
971 Science Letters 168, 27–44.
972 Petermann, M., Hirschmann, M.M., Hametner, K., Gunther, D., and Schmidt, M.W.
973 (2004) Experimental determination of trace element partitioning between garnet and
974 silica-rich liquid during anhydrous partial melting of MORB-like eclogite.
975 Geochemistry, Geophysics, Geosystems, 5, doi:10.1029/2003GC000638.
976 Pickering-Witter, J., Johnston, A.D. (2000) The effects of variable bulk composition on
977 the melting systematics of fertile peridotitic assemblages. Contributions to Mineralogy
978 and Petrology 140, 190–211.
979 Perfit, M. R., D. J. Fornari, W. I. Ridley, P. D., Kirk, J. Casey, K. A. Kastens, J. R.
980 Reynold, M. Edward, D. Desonie, R. Shuster, S. Paradis (1996) Recent volcanism in
981 the Siqueiros transform fault: picritic basalts and implications for MORB magma

Genesis. Earth and Planetary Science Letters, 14191-108.
Putirka, K. (2005) Mantle potential temperatures at Hawaii, Iceland, and the mid-ocean ridge system, as inferred from olivine phenocrysts: evidence for thermally driven mantle plumes. Geochemistry, Geophysics, Geosystems, 6, doi: 10.1029/2005GC000915.
Putirka, K. (2008) Excess temperatures at ocean islands: implications for mantle layering and convection. Geology, 36, 283-286.
Putirka, K. (2016) Rates and styles of planetary cooling on Earth, Moon, Mars, and Vesta, using new models for oxygen fugacity, ferric-ferrous ratios, olivine-liquid Fe-Mg exchange, and mantle potential temperature. American Mineralogist, 101, 819-840.
Putirka, K.D., Perfit, M., Ryerson, F.J., and Jackson, M.G. (2007) Ambient and excess mantle temperatures, olivine thermometry and active vs. passive upwelling. Chemical Geology, 241, 177-206.
Putirka, K., Ryerson, F.J., Perfit, M., and Ridley, W.I. (2011) Mineralogy and composition of the oceanic mantle. Journal of Petrology, 52, 279-313.
Prytulak, J., and Elliott, T. (2007) TiO_2 enrichment in ocean island basalts. Earth and Planetary Science Letters, 263, 388-403.
Rhodes, J. M. and Vollinger, M. J. (2004) Composition of basaltic lavas sampled by phase-2 of the Hawaii Scientific Drilling Project: geochemical stratigraphy and magma series types. Geochemistry, Geophysics, Geosystems 5, doi:10.1029/2002GC00434.
Ringwood, A.E. (1962) A model for the upper mantle. Journal of Geophysical Research, 67, 857-867.
Rizo, H., Walker, R.J., Carlson, R.W., Horan, M.F., Mukhopadhyay, S., Manthos, V., Francis, D., and Jackson, M.G. (2016) Preservation of Earth-forming events in the tungsten isotopic composition of modern flood basalts. Science, 352, 809-812.
Robinson, J.A.C., Wood, B.J., Blundy, J.D. (1998) The beginning of melting of fertile and depleted peridotite at 1.5 GPa. Earth and Planetary Science Letters 155, 97–111.
Salters, V.J.M. and Longhi, J.E. (1999) Trace element partitioning during the initial stages of melting beneath ocean ridges. Earth and Planetary Science Letters, 166, 15-30.
Salters, V.J.M. and Stracke, A. (2004) Composition of the depleted mantle. Geochemistry, Geophysics, Geosystems, 5, doi:10.1029/2003GC000597.
Sen, I.S., Bizimis, M., Sen, G., and Huang, S. (2011) A radiogenic Os component in the oceanic lithosphere? Constraints from Hawaiian pyroxenite xenoliths. Geochemica et Cosmochimica Acta, 75, 4899-4916.
Shea, T., Costa, F., Krimer, D., and Hammer, J.E. (2015a) Accuracy of timescales retrieved from diffusion modeling in olivine: a 3D perspective. American Mineralogist, 100, 202602042.
Shea, T., Lynn, K.J., and Garcia, M.O. (2015b) Cracking the olivine zoning code: distinguishing between crystal growth and diffusion. Geology, 43, 935-938.
Shimizu, K., Saal, A. E., Myers, C. E., Nagle, A. N., Hauri, E. H., Forsyth, D. W., ... & Niu, Y. (2016). Two-component mantle melting-mixing model for the generation of mid-ocean ridge basalts: Implications for the volatile content of the Pacific upper mantle. Geochimica et Cosmochimica Acta, *176*, 44-80.

1028 Siebert, J. Corgne, A. and Ryerson, F.J. (2011) Systematics of metal-silicate partitioning
1029 for many siderophile elements applied to Earth's core formation. Geochimica et
1030 Cosmochimica Acta, 75, 1451-1489.
1031 Sobolev, et al. (2007) The amount of recycled crust in source of mantle-derived melts.
1032 Science, 316, 412-417.
1033 Starkey, N. Fitton, J.G., Stuart, F.M., and Larson, L.M. (2012) Melt inclusions in olivines
1034 from early Iceland plume picrites support high $^{3}He/^{4}He$ in both enriched and depleted
1035 mantle. Chemical Geology, 306, 54-62.
1036 Stuart, F.M., Lass-Evans, S., Fitton, J.G., and Ellam, R.M. (2003) High $^{3}He/^{4}He$ ratios in
1037 picritic basalts from Baffin Island and the role of a mixed reservoir in mantle plumes.
1038 Nature, 424, 57-59.
1039 Stolper, E. (1980) A phase diagram for mid-ocean ridge basalts: preliminary results and
1040 implications for petrogenesis. Contributions to Mineralogy and Petrology, 74, 13-27.
1041 Stormer, J.C. (1973) Calcium zoning in olivine and its relationship to silica activity and
1042 pressure. Geochimica et Cosmochimica Acta, 37, 1815-1821.
1043 Stracke, A. (2012) Earth's heterogeneous mantle: a product of convection-driven
1044 interaction between crust and mantle. Chemical Geology, 330-331, 274-299.
1045 Takahashi, E., and Kushiro, I. (1983) Melting of a dry peridotite at high pressures and
1046 basalt magma genesis. American Mineralogist, 68, 859-879.
1047 Takahashi, E., Shimazaki, T., Tsuzaki, Y., Yoshida, H. (1993) Melting study of a
1048 peridotite KLB-1 to 6.5 GPa, and the origin of basaltic magmas. Philosophical
1049 Transactions of the Royal Society of London 342, 105–120.
1050 Tao, Y., Putirka, K., Hu, R-Z., and li, C. (2015) The magma plumbing system of the
1051 Emeishan large igneous province and its role in basaltic magma differentiation in a
1052 continental setting. American Mineralogist, 100, 2509-2517.
1053 Taura, H., Yurimoto, H., Jurita, K., and Sueno, S. (1998) Pressure-dependence on
1054 partition coefficients for trace elements between olivine and coexisting melts. Physics
1055 and Chemistry of Minerals, 25, 469-484.
1056 Thomson, A. and Maclennan, J. (2013)The distribution of olivine compositions in
1057 Icelandic basalts and picrites. Journal of Petrology, 54, 745-768.
1058 Tsuno, K., and Dasgupta, R. (2011) Melting phase relations of nominally anhydrous,
1059 carbonated politic-eclogite at 2.5-3.0 GPa and deep cycling of sedimentary carbon.
1060 Contributions to Mineralogy and Petrology, 161, 743-763.
1061 Walter, M.J. (1998) Melting of garnet peridotite and the origin of komatiite and depleted
1062 lithosphere. Journal of Petrology 39, 29–60.
1063 Wang, Z. and Gaetani, G.A. (2008) Partitioning of Ni between olivine and siliceous
1064 eclogite partial melt: experimental constraints on the mantle source of Hawaiian
1065 basalts. Contributions to Mineralogy and Petrology, 156, 661-678.
1066 Waters, C. L., Sims, K. W., Perfit, M. R., Blichert-Toft, J., & Blusztajn, J. (2011)
1067 Perspective on the genesis of E-MORB from chemical and isotopic heterogeneity at
1068 9–10 N East Pacific Rise. *Journal of Petrology*, *52*(3), 565-602.
1069 White, W.M. (2015) Probing the Earth's deep interior through geochemistry.
1070 Geochemical Perspectives, 4, 1-251.
1071 Willbold, M. and Stracke, A. (2006) Trace element composition of mantle end-members:
1072 implications for recycling of oceanic and upper and lower continental crust.
1073 Geochemistry, Geophysics, Geosystems, 7, doi: 10.1029/2005GC001005.

Workman, R.K. and Hart, S.R. (2005) Major and trace element composition of the depleted MORB mantle (DMM). Earth and Planetary Science Letters, 231, 53-72.
Wright, T.L., and Fiske, R.S. (1971) Origin of the differentiated and hybrid lavas of Kilauea volcano, Hawaii. Journal of Petrology, 12, 1-65.
Wyession, M.E. (1996) Imaging cold rock at the base of the mantle: the sometimes fate of slabs? In: Bebout, G.E., Scholl, D.W., Kirby, S.H., and Platt, J.P., eds., Subduction: Top to Bottom, Geophysical Monograph 96, American Geophysical Union, p. 369-383.
Zhang, L., Smyth, J., Allaz, J., Kawazoie, T., Jacobsen, S.D., and Jin, Z. (2016) Transition metals in the transition zone: crystal chemistry of minor element substitution in wadsleyite. American Mineralogist, 101, 2322-2330.
Zhao, C., Garnero, E.J., McNamara, A.K., Schmerr, N., and Carlson, R.W. (2015) Seismic evidence for a chemically distinct thermochemical reservoir in Earth's deep mantle beneath Hawaii. Earth and Planetary Science Letters, 426, 143-153.
Zindler, A., and Hart, S. (1986) Chemical geodynamics. Annual Review of Earth and Planetary Science, 14, 493-571.

Figures

Figure 1. Weight % MgO for MORB (East Pacific Rise, Siqueiros) and Hawaiian (HSDP2; Rhodes and Vollinger 2004) whole rocks are compared to (A) FeO, (B) MnO, (C) FeO/MnO and (D) TiO_2. Whole rock compositions are also compared to liquids from peridotite partial melting experiments, sorted by pressure and using depleted and pyrolite mantle model peridotites from Takahashi and Kushiro (1983; KLB-1); Takahashi et al. (1993, KLB-1); Baker et al. (1995, MM3); Herzberg and Zhang (1996, KLB-1); Walter (1998, KR4003); Longhi (2002, Model Depleted and Primitive Upper Mantle, DPUM and PUM). Highlighted with a beige fill are 20-30 kbar partial melts of a high FeO peridotite from Kushiro (1996, PHN1611), noted as "fertile" but lower in Al_2O_3 and CaO than the other peridotites noted. Plume model 1 is a 50-50 mixture of Walter (1998; 45 kbar, 1620°C) and Kushiro (1996; 30 bar, 1460°C). Plume model 2 is a 40-60 mixture of peridotite partial melts from Takahashi and Kushiro (1983; 35 kbar, 1600°C), and Walter (1998; 45 kbar, 1620°C). The MORB model is a 56-44 mixture of Kushiro (1996; 10 kbar, 1360°C), and Baker et al. (1995; 10 kbar, 1280°C).

Figure 2. Trace element concentrations in Fo89 olivine, from average or projected values, normalized to Fo89 olivine compositions from MORB (Siqueiros). From Ca to Mn, elements are listed in order of increasing Ol/Liq partition coefficients (element [*D*]): Ca [0.01], Ti [0.01], Al [0.015], Na [0.015], Cu [0.1], Sc [0.2], Mn [0.9]. From Mn to P, elements are listed in order of increasing core/mantle partitioning using the mid-point of minimum and maximum values of Siebert et al. (2011; their Table 6) (element [*D*]): Mn [1], V [1.9], Cr [3], Zn [4], Co [24.5, Ni [26], P [35].

Figure 3. Comparison of the highly incompatible elements (in Ol), Ti (A) and (B) and Sc (C) and (D) for host liquids and olivine grains (data from GEOROC; http://georoc.mpch-mainz.gwdg.de/georoc/); Hawaii (Rhodes and Vollinger 2004); MORB (PetDB; http://www.earthchem.org/petdb). Black curves are high-T plume LLD and CLDs; gray

curves are low-T mid-ocean ridge LLD and CLDs (see text for discussion and calculation details). We find that an enriched mantle source and very low partition coefficients for Ti are required to simultaneously explain Ti in whole rocks and co-existing olivine; see text for discussion. Symbols as in Fig. 2; D_{Ti} = exp(-5.2 + 1979/[T°C], initial TiO_2^{liq} = 1.6 wt. % or 9592 ppm Ti, at 20% MgO^{liq}; T(°C) = 1014+20.1[MgO^{liq}].

Figure 4. Comparison of compatible elements (Ol-liq partition coefficients near 1.0), Mn (A) and (B), Zn (C) and (D) and Cr (E) and (F), for published whole rocks (putative liquids; see caption to Fig. 3) and our new data for olivine grains. When $D_i^{ol\text{-}liq}$ is close to 1, the trace element contents of Ol can be quite sensitive to T. For example, in Mn and Zn, liquid compositions don't vary at MgO^{liq}>10%, and yet Zn-in-Ol and Mn-in-Ol increase greatly, as $D_i^{ol\text{-}liq}$ increases (from slightly <1 to slightly > 1) with decreasing T. On the other hand, Cr-in-Ol mostly decreases as MgO decreases, as other phases (most likely spinel) deplete coexisting liquids in Cr. Symbols as in Fig. 2. D_{Cr} = exp(-2.51 + 3003.7/[T°C], initial Cr^{liq} = 680 ppm at 20% MgO^{liq}; D_{Mn} = exp(-3.6 + 4500/[T°C], initial MnO^{liq} = 0.17 wt. % at 18% MgO^{liq}; see caption to Fig. 3 for similar calculations of LLD and CLD curves (black for plume, gray for MORs). Curves are not shown for Zn, as current partitioning experiments are too few and fail to reproduce Zn-in-Ol trends.

Figure 5. (A) Whole rock Ni (ppm) vs. MgO (wt. %) compositions from Emeishan, Baffin Island, Deccan and MORB (see caption to Fig. 3). (B) Whole rock Hawaii and MORB compositions are compared to olivine compositions from Putirka et al. (2011). (C) Histogram of Hawaiian Ol compositions; (D) Cation fractions of MgO and FeO in Hawaiian whole rocks (triangles), with isopleths that show the positions of liquids in equilibrium with a given Fo content, when $K_D(Fe\text{-}Mg)^{ol\text{-}liq}$ = 0.34; isotherms are from Putirka (2005); red circles indicate Hawaiian liquids needed to produce maximum, minimum and median Ol compositions in panel C; dashed line in D shows the position of Hawaiian glass compositions. Other symbols as in Fig. 2. In (A), it is clear that at a given MgO content, Ni contents for plumes are not enriched relative to MORB. In (B), whole rock Ni contents at MgO>21%, are controlled by mixing with Ol, which likely explains subtle contrasts between Ni contents at Baffin compared to Emeishan, Hawaii or Deccan in panel (A). Panel (D), with isotherms and Ol isopleths from Putirka (2005), similarly shows the range of liquids required to produce observed Hawaiian Ol compositions (gray area, Fo71.7-Fo90.5, as in panel C). Such liquids must have up to 20.8% MgO, with a continuum down to 6.3% MgO, to create the continuum of Ol compositions in panel C.

Figure 6. (A) New data for Olivine Ni v. Forsterite (Fo) contents. (B) and (C) Whole rock Ni v. MgO. (D) New Cr vs. Ni in Ol compositions. Symbols are as in Fig. 2; whole rock data are as in Fig. 3 caption; see electronic supplement for new Ol data . Panels (A) and (B) show models that explain high Ni-in-Ol at moderate to low Fo (≤Fo88). For (A) and (B) Crystal Lines of Descent (CLDs) and Liquid Lines of Descent (LLDs) are calculated by selecting as starting compositions, MgO^{liq}-Ni^{Liq} values that fall on the observed whole rock trends of (B), and then subtracting calculated Ol compositions in 2% increments using mass balance. Gray curves use Eqn. (1e), black and red curves Eqn. 1b, and the blue curve Eqn. (1c); in panel (A) we use Eqn. (3) to obtain Fo contents in Ol;

in panel (B) we use Eqn. (4) for $FeOt^{liq}$ = 11.5 wt.% to obtain MgO^{Ol}, and then calculate MgO^{liq} from mass balance. To evaluate all of Eqns. (1b,e,c), (3) and (4), T is re-calculated at each step using Helz and Thornber (1987) [$T(^oC) = 20.1[MgO^{liq}] + 1014$] for both MORB and Hawaiian lavas, although a separate calibration for MORB, $T(^oC) = 17.5[MgO^{liq}] + 1054$ (calibrated from Bender et al. 1984; Grove and Juster 1989; Grove and Bryan 1983) yields similar results at high T. Dashed curves are "failed" models: they explain some Ni vs. Fo trends in olivine, but not Ni vs. MgO in whole rocks (nominal liquids) or Liq + Ol mixtures (see Fig. 5B for Liq + Ol trajectories). Green dashed curve is a modified version of the Cpx-dominated CLD and LLD from Putirka et al. (2011), while red dashed curve uses Eqn. (1b) and assumes that high Ni in Fo88 olivine derives from a Ni-enriched liquid. Predicting observed Ni contents for olivines with <Fo88 yield coexisting liquids displaced even further from observed whole rock trends. In (C), we show the difficulty of explaining whole rock Ni contents if we assume Ni-enriched parent liquids: the red curve from (B) is reproduced as Ol LLD1 (with 1500 ppm Ni at 20% MgO), and is compared to Ol LLD2, which uses the same starting liquid, but uses Eqn. 1c and the thermometer of Putirka (2008), and Ol LLD3, which uses Eqn. 1a with the Helz and Thornber (1987) thermometer, and a liquid with 1200 ppm Ni at 20% MgO; each model successfully predicts Ni-in-Ol at Fo88, but fails to reproduce Ni contents of whole rocks. The models are derived assuming that Ol precipitates from melts derived by partial melting of pyroxenite (gray curves) or peridotite (green curves). Le Roux et al. (2011) suggest that $D_{Ni}^{Cpx\text{-}liq} = 22$ in some circumstances, but we see little evidence for such high values in experimental data, and we find that $D_{Ni}^{Cpx\text{-}liq} = 3$ fits observed Ni-in-Ol compositions much better (see discussion for details).

Figure 7. Magnified view of Hawaiian (and Siqueiros) samples as in Figure 5, to compare olivine Ni v Fo (A), and whole rock Ni vs. MgO (B), for olivines with moderate Fo contents but high Ni. Olivine grains at ≤ Fo88 cannot form from Ni-enriched magmas—such magmas do not exist (Fig. 6B). But they can from observed liquids (B) at lower temperatures (where D_{Ni} is elevated) that are Fe-rich (which decreases Fo at a given MgO^{liq}). To determine these liquids, we take those Ol grains with the highest NiO at a given Fo content (empirically, $Ni_{max}^{Ol}(ppm) = 65.8[Fo] - 2271$, and $Fo = 100[(X_{MgO}^{Ol}/(X_{MgO}^{Ol}+X_{FeO}^{Ol})])$ and then use Fo to calculate MgO^{liq}, which (in a variation of Eqn. 4) can be found empirically, if $FeOt^{liq}$ is known: for $FeOt^{liq}$ = 13 wt. %, $MgO^{liq} = (0.603 - 0.0061[Fo])^{-1}$; for $FeOt^{liq}$ = 18 wt. %, $MgO^{liq} = (0.383 - 0.0039[Fo])^{-1}$); Ni-in-liq can be determined from the whole rock trend: $Ni^{liq}(ppm) = 63.3MgO^{liq}-364.8$. These calculations provide what we need to determine D_{Ni} –in effect forcing the high Ni Ol crystals (orange circles in panel A) to form from liquid compositions in panel (B) (orange circles), connected by straight lines. Having D_{Ni}, and MgO^{liq}, the tables in (A) use such as input to compare the implied T using Helz and Thornber (1987) with the T implied from D_{Ni} using Eqn. (2). Temperature estimates are close at high MgO, but diverge as MgO decreases, where an olivine with Fo73 and 2,530 ppm Ni requires an impossibly high D_{Ni} (=59) and low T^{Ni} (<900°C). But rare Hawaiian samples range to 18 wt. % FeOt; in such a liquid this same olivine can form from MgO^{liq} = 10.2 wt. %, with a resulting D_{Ni} = 9.1 and temperature estimates coincide within error. Black and gray curves in (B) are batch partial melts, $C_{Ni}^{liq} = C_{Ni}^{source}/[F + D^{bulk}(1\text{-}F)]$, where C_{Ni}^{source} = 1900 (for a peridotite source; Sobolev et al. 2007). Melt compositions are calculated at 25°C above the solidus

(Hirschmann 2000), which approximates a melt fraction (F) of 10% (e.g., Baker et al. 1995). We calculate MgO^{liq} (wt. %) = -55.96 + 0.0532[T(°C)] -2.16[P(GPa)], using this "solidus + 25°C" curve as input; this expression for MgO^{liq} reproduces calibration data (Takahashi et al. 1993; Baker et al. 1995; Herzberg and Zhang 1996; Kushiro 1996; Robinson et al. 1998; Walter 1998; Pickering-Witter and Johnston 2000) to ±2 wt. %. For Ni-in-Liq we use F = 0.1, and D^{bulk} assumes: 20% Opx, 15% Cpx and 65% Ol, $D_{Ni}^{cpx\text{-}liq}$ = 3.2 and $D_{Ni}^{opx\text{-}liq}$ = 3.7 (from Le Roux et al. 2015). For $D_{Ni}^{ol\text{-}liq}$, the gray curve uses Eqn. (1a) and the black curve uses (1b).

Figure 8. A comparison of CaO (A and B) and Al or Al_2O_3 (C and D) between whole rock MgO (see Fig. 3 caption) and Fo from new olivine compositions (see electronic supplements). In (E) and (F), Ni in Ol is compared to Ca and Al in Ol respectively from these same data sets. The experimentally-derived MORB and Plume model 2 peridotite partial melts are determined as in the caption to Fig 1. (A) and (C) show that MORB have higher CaO and Al_2O_3 compared to plume derived lavas, and that in both cases, such contrasts likely result from contrasts in melting conditions of a peridotite source. Such partial melts with low Al_2O_3 are mostly garnet saturated, indicating that deep-seated partial melting, within the garnet stability field, is much more important at Hawaii, Emeishan and Deccan, compared to Baffin or MORB. Olivine Ca and Al concentrations reflect these contrasts in liquid composition. Also plotted in (B) is the field of Ca for olivines precipitated from experimental pyroxenite partial melts, from Kogiso et al. (1998), Kogiso and Hirschmann (2001) and Lambart et al. (2009). Only the Ca contents of olivine from Emeishan and Deccan are consistent with a pyroxenite derivation. But all natural plume-derived olivine grains have vastly more Al than expected compared to pyroxenite-melt equilibrated Ol from Lambart et al. (2009) (D).

Figure 9. The trace element concentrations in our selected plume sources are calculated from parental magma compositions (see appendix tables 2 and 3) as in Putirka et al. (2011), and normalized to (A) our MORB-source mantle ("MORB-Siqueiros"; calculated from Siqueiros parental magmas) and (B) various estimates of depleted and pyrolite mantle, where "Pyrolite(M&S)" is the pyrolite model of McDonough and Sun (20015); "Baffin" is our estimate of the Baffin Island source; "DMM (W&H)" is "depleted MORB mantle of Workman and Hart (2005); and "DM(S&S) is the MORB Depleted mantle source of Salters and Stracke (2004). The pyrolite model of Lyubetskaya and Korenaga (2010) is not plotted, but is effectively identical to the curve for McDonough and Sun (1995). The "anticipated" errors are calculated as the maximum – minimum (range) normalized concentration ratios, calculated using maximum and minimum ranges of F at both MORB and Hawaii, and maximum and minimum partition coefficients for MORB and Hawaii, as in Putirka et al. (2011) (i.e., the highest normalized ratio for Th is that obtained by allowing F at Hawaii to be 0.25, so requiring more Th in the Hawaiian source, and using F = 0.08 for MORB, to minimize calculated Th in the MORB source). As noted in the text, our Cr estimate for DM (1,100 ppm) is much lower than Salters and Stracke (2004; 2,500 ppm). We assume 600 ppm in mantle-equilibrated MORB (Fig. 4E), and a bulk D_{Cr} during mantle melting of 1.92. We can obtain 2,500 ppm by increasing Cr^{liq} to

1400 ppm, which seems vastly too high compared to primitive MORB, or by increasing bulk D_{Cr} to 4.5, which can only be reached or exceeded in garnet at high T and would require very high residual garnet in the source (e.g., Putirka 1998).

Figure 10. (A) Our Hawaiian trace element source is compared to our model plume sources, obtained by mixing MORB crust with depleted MORB-source mantle (effectively the "pyrolite" of Ringwood (1962)). "HMS" = Hawaiian mantle source. "SMS" is our depleted Siqueiros mantle source (appendix Table 3); "DM1" is depleted mantle from Workman and Hart (2005); "DM2" is depleted mantle from Salters and Stracke (2004); "BMS" is our calculated Baffin mantle source. The models that make use of DM1 and BMS depleted mantles are mixed with ocean crust that is equal to the mean MORB estimate of Gale et al. 2013), while the DM and DM2 models are mixed with MORB from Putirka et al. (2011). (B) Our calculated depleted mantle source for Baffin Island (BMS) is compared directly to SMS, DM1, DM2 as in panel (A), and the pyrolite model of McDonough and Sun (1995).

Table 1. Estimates of mantle potential temperature and related inp

Plumes and MORB	***Tp*** **(°C) (1)**	**Source Olivine Fo (2)**
Emeishan (Low Ti)	1700(67)	92.5
Emeishan (High Ti)	1480(84)	89.5
Deccan (H&G 2009)	1620(54)	91.5
Hawaii (SR0061-0)	1630(77)	91.0
Baffin (Hole 2015)	1630(65)	92.0
MORB-Siqueiros	1420(40)	91.4
MORB Mean Mean Cottlrell and Kelley (2011)	1320(39)	89.3
Other plume and MORB estimates		
Siberian Traps	1590(37)	92.0
Ferropicrites	1780(155)	92.0
Samoa	1620(66)	91.7
Iceland	1520(46)	91.7
MORB, 9°N; Cottrell & Kelley (2011)	1400(37)	90.5
MORB (Herzberg)	1400(38)	91.3
MORB Cottrell and Kelley	1390(45)	90.7

Notes: (1) Tp = mantle potential temperture; Tp is calculated as in Putirka (20
(2) Olivine forsterite (Fo) contents are calculated from liquid compositions usir
Olivine and liquid compositions are not arbitrary. Liquid compositions are sele

ɔut parameters

Putirka (2008) Eqn. 42 P (GPa)	log[fO_2] at NNO	Putirka (2016) Eqn. 8b $K_D(Fe\text{-}Mg)^{ol\text{-}liq}$	$T^{ol\text{-}liq}$ Putirka et al. (2007) T (^oC)
3.23	-3.18	0.350	1597
2.05	-4.51	0.342	1468
2.63	-3.78	0.347	1539
2.51	-3.75	0.349	1549
2.41	-4.05	0.347	1512
1.59	-5.38	0.342	1376
1.14	-6.17	0.341	1311
2.26	-4.18	0.347	1502
3.96	-2.32	0.347	1696
3.16	-3.27	0.347	1582
1.97	-4.71	0.344	1447
1.39	-5.60	0.342	1363
1.55	-5.49	0.342	1367
1.50	-5.52	0.340	1392

16); see electronic appendix for input liquid compositions, and olivine + liquid temperat
ıg the calculated oxygen fugacity, and Fe3+/Fe2+ ratios as determined using equation
cted so that the calculated Fo contents for olivine match observed maximum Fo conte

Melt Fraction Putirka (2016) Avg. Eqns. 14a-c
0.233(0.042)
0.066(0.054)
0.183(.004)
0.189(0.009)
0.239(0.041)
0.106(0.028)
0.032(0.029)
0.189(0.017)
0.212(0.095)
0.136(0.024)
0.158(0.027)
0.091(0.005)
0.097(0.026)
0.069(0.022)

tures
ıs in Putirka (2016).
nts of high Ca olivine phenocrysts.

Figure 1

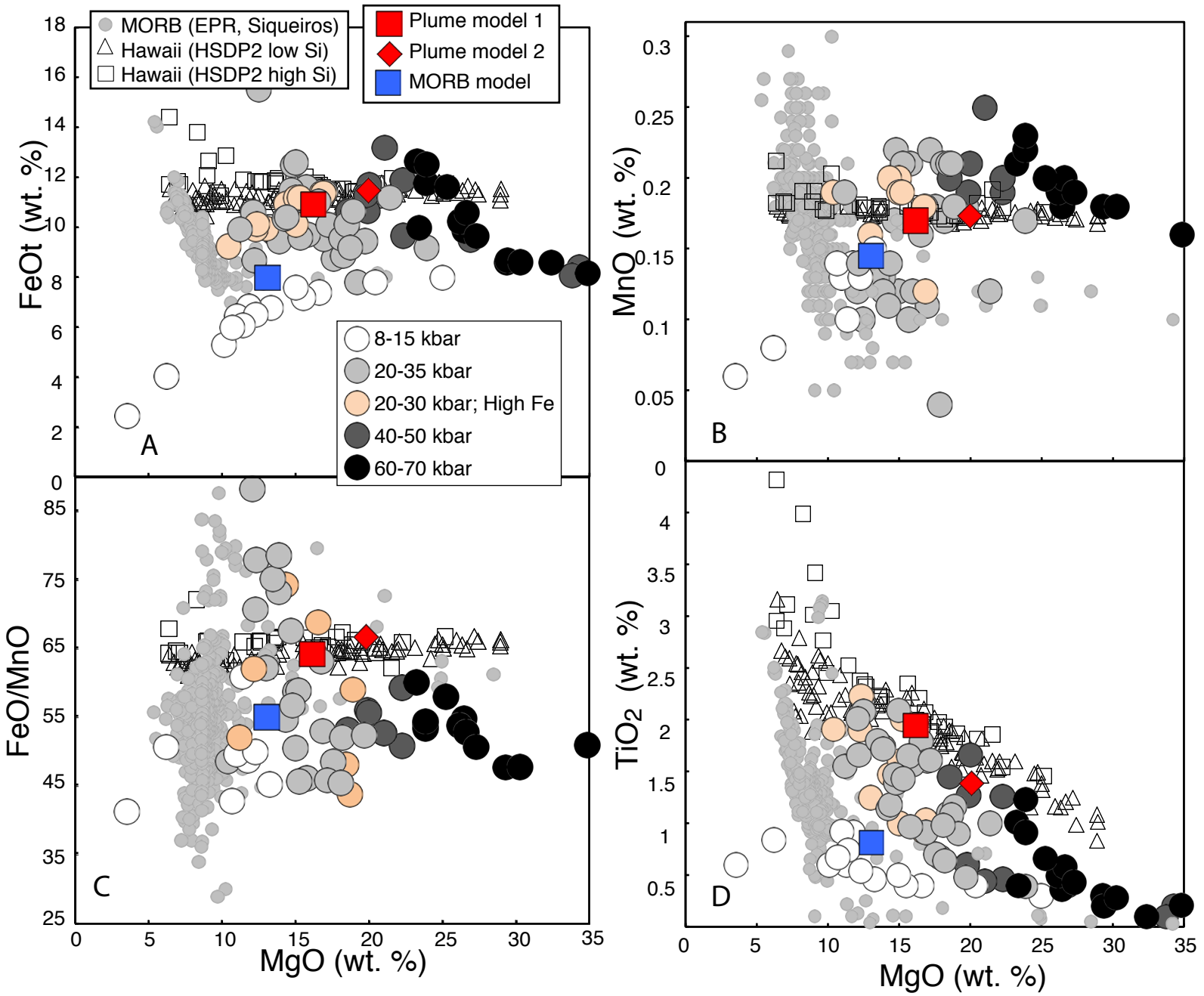
MORB (EPR, Siqueiros)
Hawaii (HSDP2 low Si)
Hawaii (HSDP2 high Si)
Plume model 1
Plume model 2
MORB model
8-15 kbar
20-35 kbar
20-30 kbar; High Fe
40-50 kbar
60-70 kbar
A
B
C
D
FeOt (wt. %)
MnO (wt. %)
FeO/MnO
TiO2 (wt. %)
MgO (wt. %)
MgO (wt. %)

Figure 2

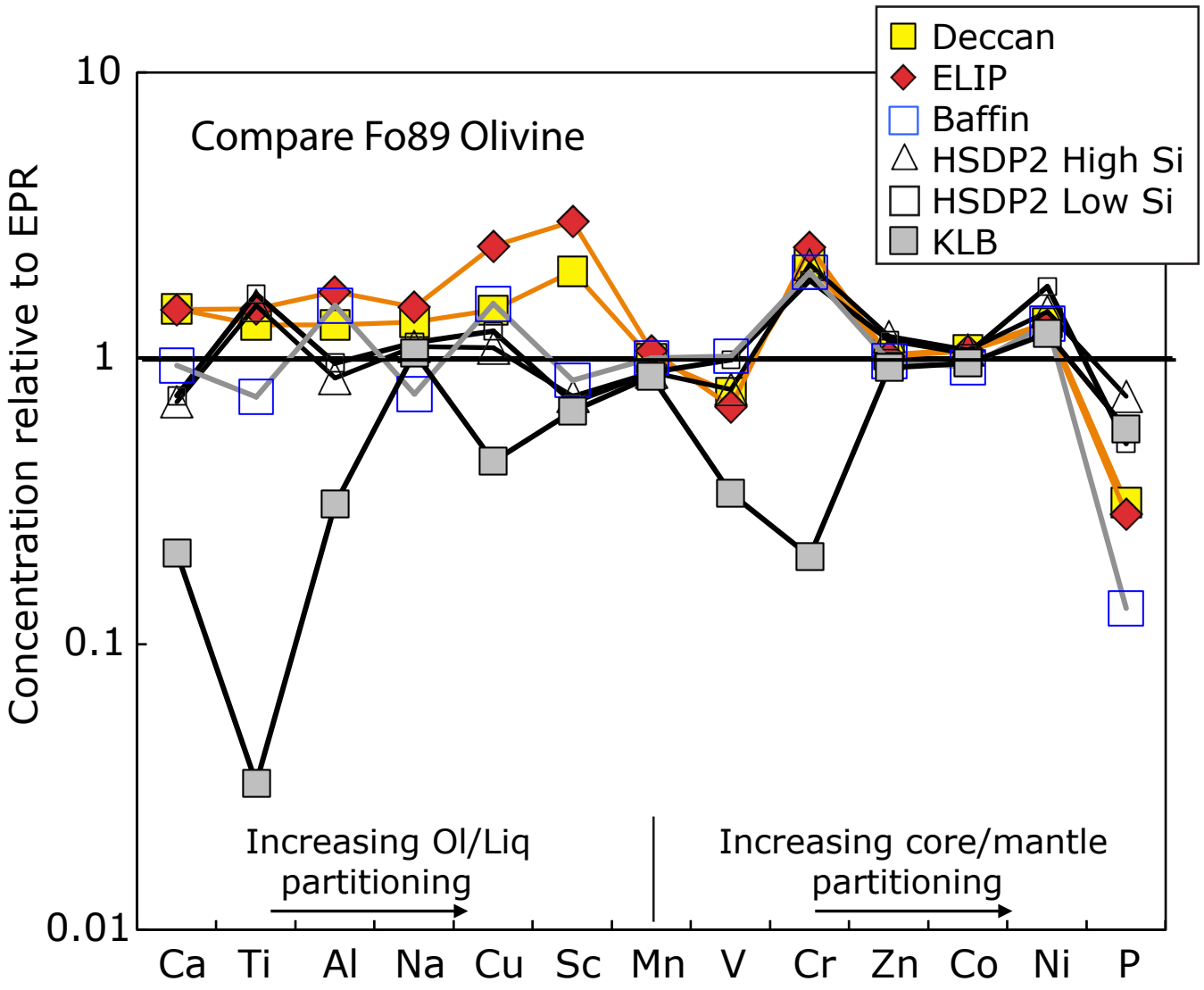
Deccan
ELIP
Baffin
HSDP2 High Si
HSDP2 Low Si
KLB
Compare Fo89 Olivine
Concentration relative to EPR
10
1
0.1
0.01
Increasing Ol/Liq partitioning
Increasing core/mantle partitioning
Ca
Ti
Al
Na
Cu
Sc
Mn
V
Cr
Zn
Co
Ni
P

Figure 3

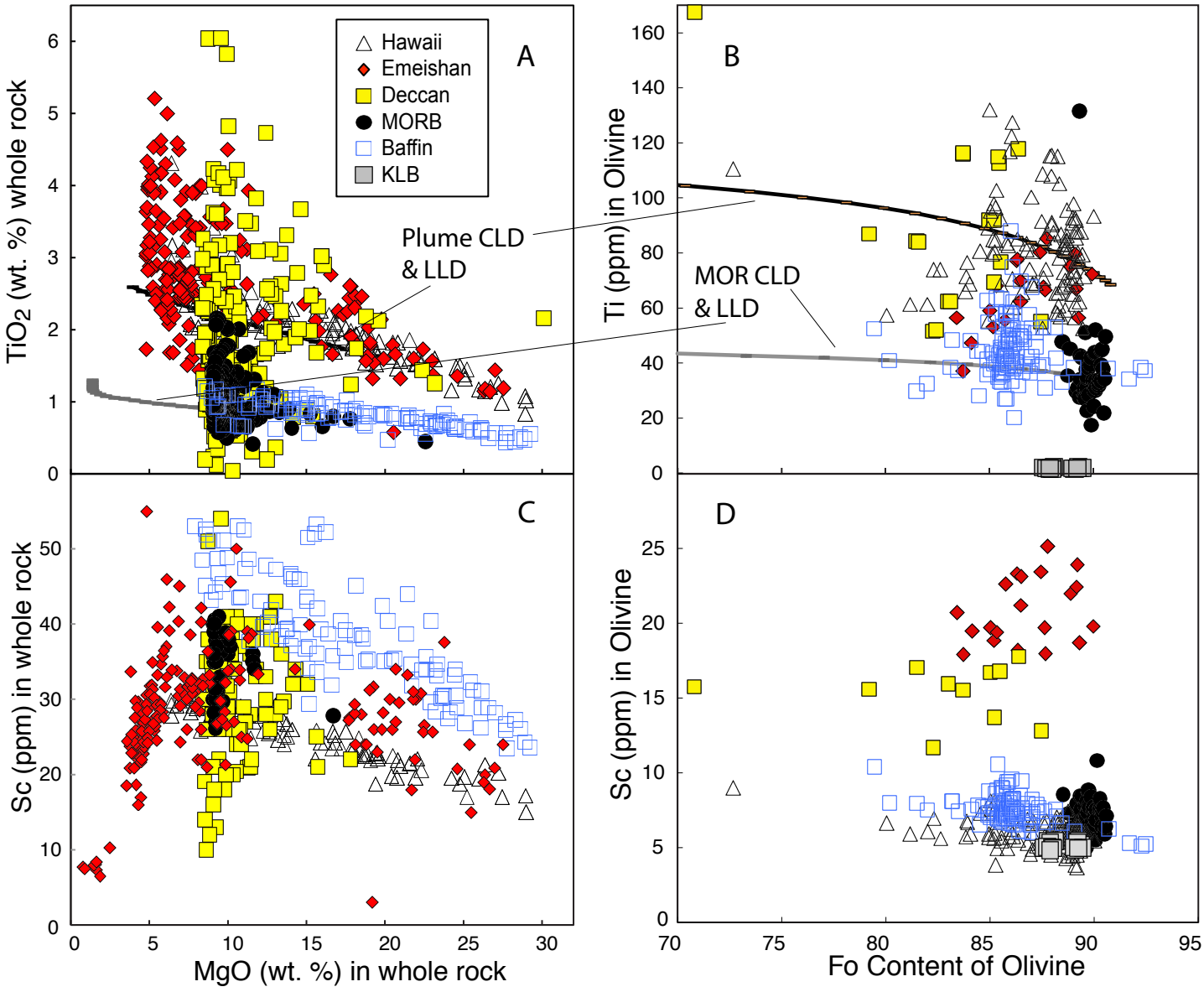
A
B
C
D
Hawaii
Emeishan
Deccan
MORB
Baffin
KLB
Plume CLD
& LLD
MOR CLD
& LLD
TiO2 (wt. %) whole rock
Ti (ppm) in Olivine
Sc (ppm) in whole rock
Sc (ppm) in Olivine
MgO (wt. %) in whole rock
Fo Content of Olivine

Figure 4

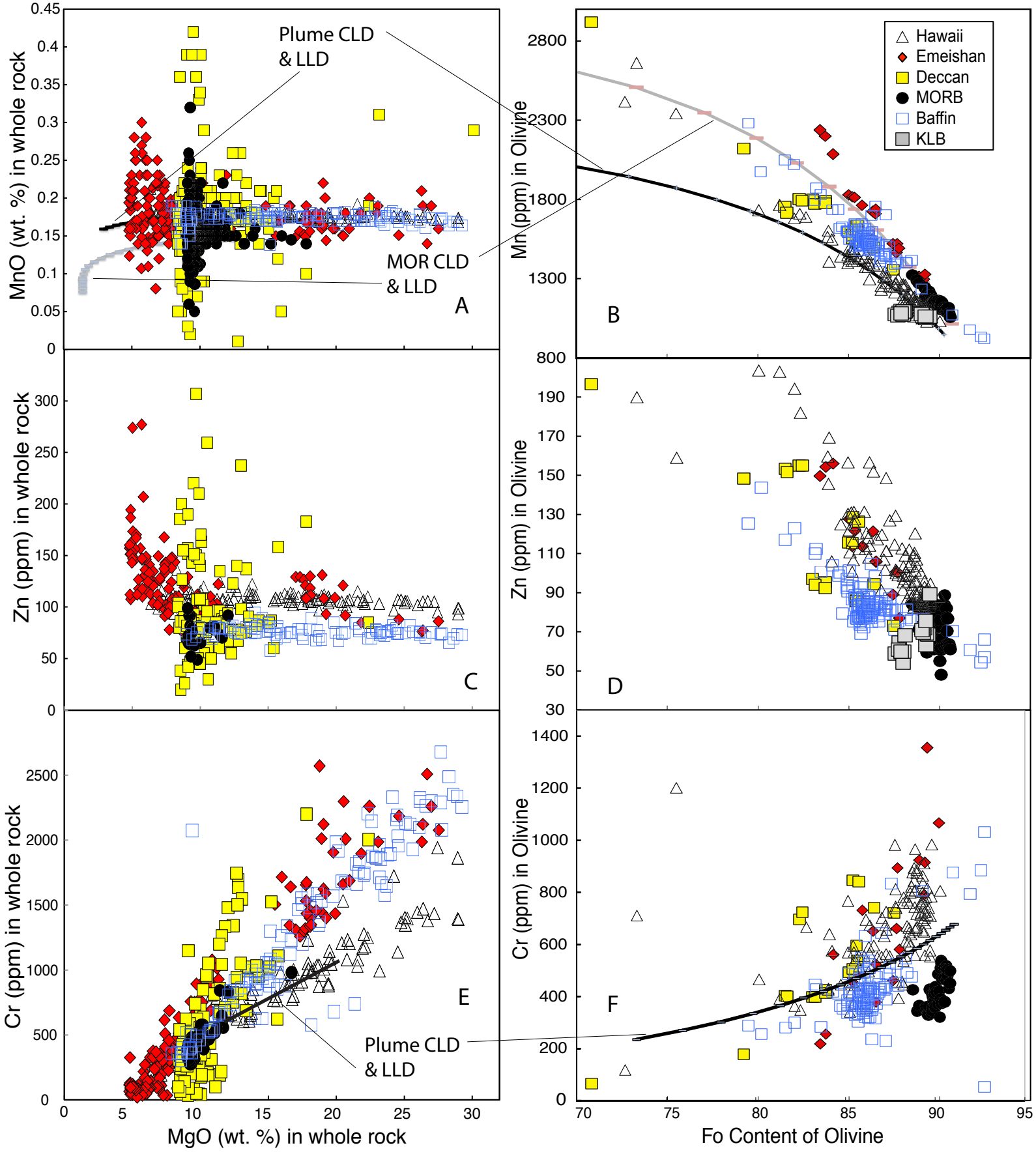
MnO (wt. %) in whole rock
Plume CLD & LLD
MOR CLD & LLD
A
Mn (ppm) in Olivine
Hawaii
Emeishan
Deccan
MORB
Baffin
KLB
B
Zn (ppm) in whole rock
C
Zn (ppm) in Olivine
D
Cr (ppm) in whole rock
E
Plume CLD & LLD
Cr (ppm) in Olivine
F
MgO (wt. %) in whole rock
Fo Content of Olivine

Figure 5

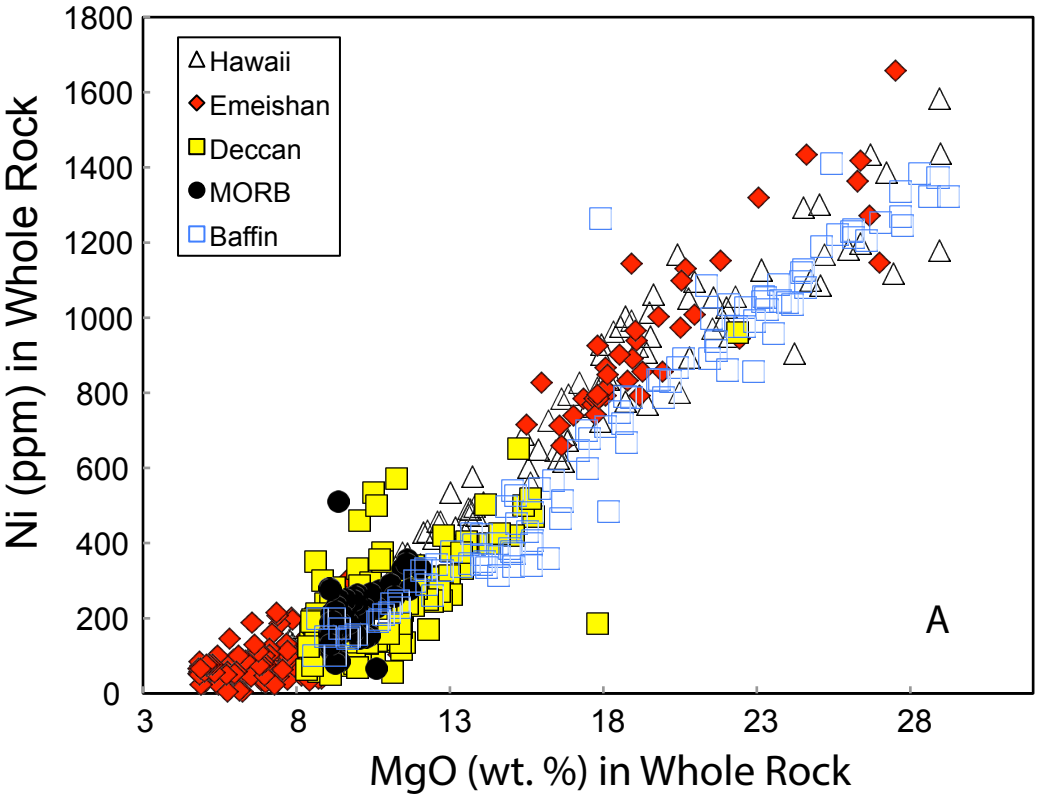
Hawaii
Emeishan
Deccan
MORB
Baffin
Ni (ppm) in Whole Rock
MgO (wt. %) in Whole Rock
A

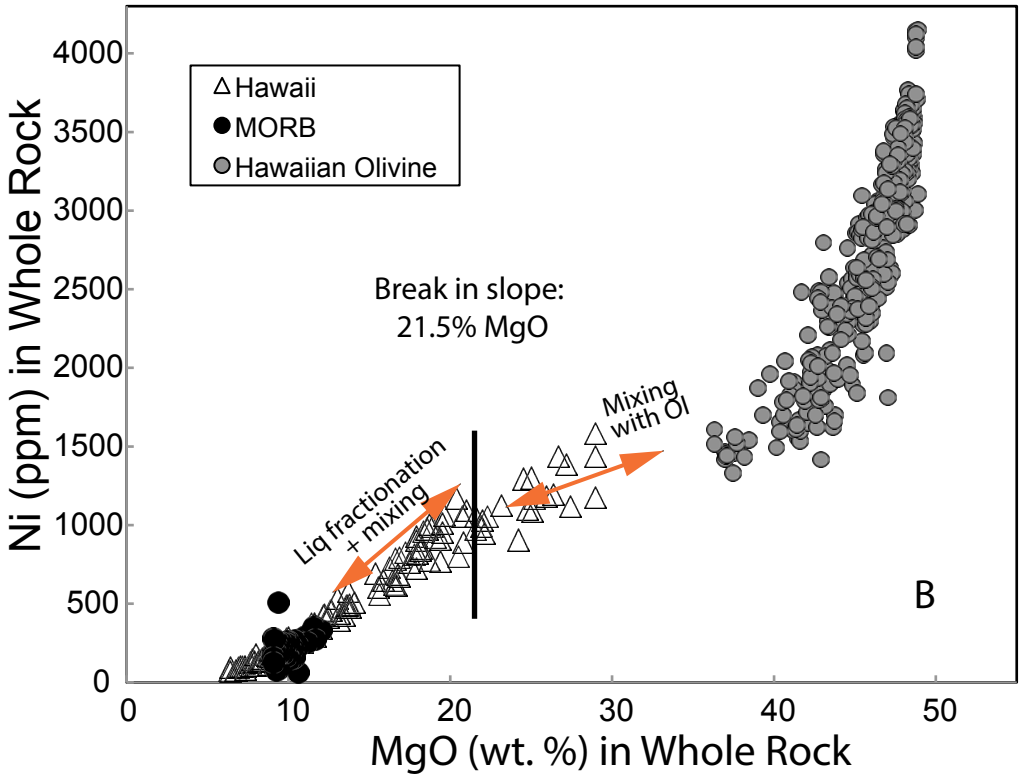
Hawaii
MORB
Hawaiian Olivine
Break in slope:
21.5% MgO
Liq fractionation
+ mixing
Mixing
with Ol
Ni (ppm) in Whole Rock
MgO (wt. %) in Whole Rock
B

Figure 6E

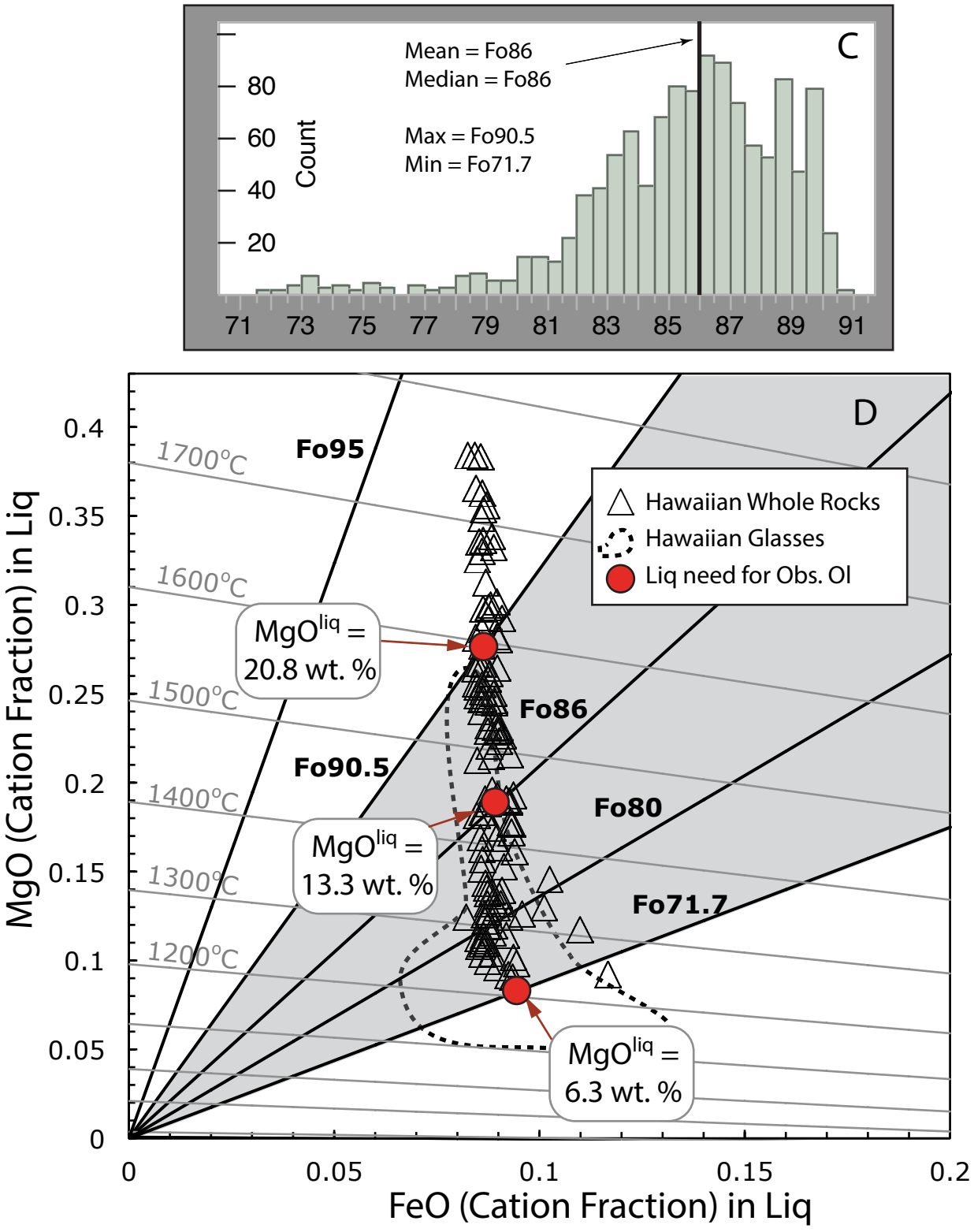
C
Mean = Fo86
Median = Fo86
Max = Fo90.5
Min = Fo71.7
Count
80
60
40
20
71
73
75
77
79
81
83
85
87
89
91
D
Fo95
Fo90.5
Fo86
Fo80
Fo71.7
1700°C
1600°C
1500°C
1400°C
1300°C
1200°C
Hawaiian Whole Rocks
Hawaiian Glasses
Liq need for Obs. Ol
MgO^liq = 20.8 wt. %
MgO^liq = 13.3 wt. %
MgO^liq = 6.3 wt. %
MgO (Cation Fraction) in Liq
FeO (Cation Fraction) in Liq
0
0.05
0.1
0.15
0.2
0.25
0.3
0.35
0.4

Figure 6

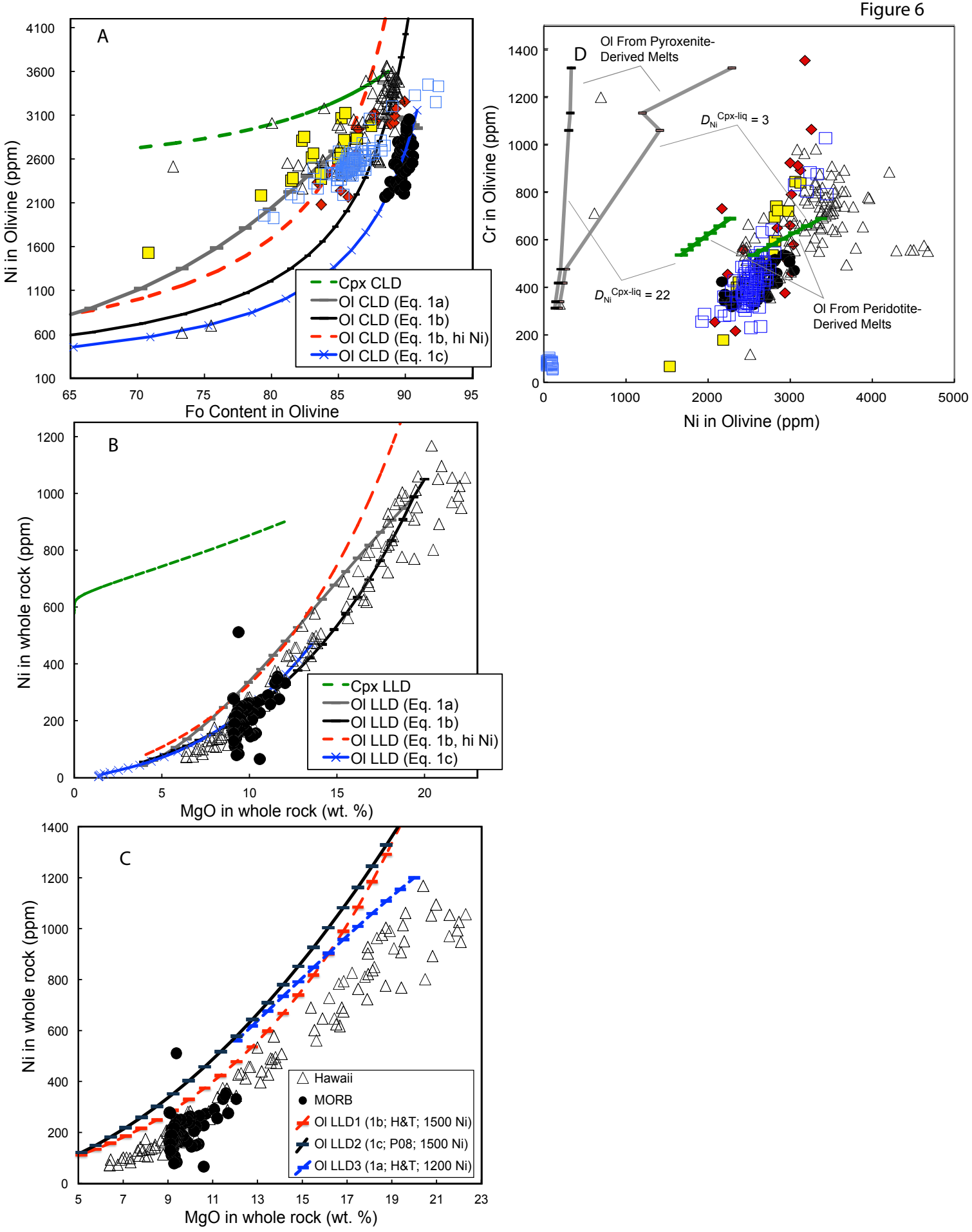
A
Ni in Olivine (ppm)
Fo Content in Olivine
Cpx CLD
Ol CLD (Eq. 1a)
Ol CLD (Eq. 1b)
Ol CLD (Eq. 1b, hi Ni)
Ol CLD (Eq. 1c)
D
Ol From Pyroxenite-Derived Melts
$D_{Ni}^{Cpx-liq}$ = 3
$D_{Ni}^{Cpx-liq}$ = 22
Ol From Peridotite-Derived Melts
Cr in Olivine (ppm)
Ni in Olivine (ppm)
B
Ni in whole rock (ppm)
MgO in whole rock (wt. %)
Cpx LLD
Ol LLD (Eq. 1a)
Ol LLD (Eq. 1b)
Ol LLD (Eq. 1b, hi Ni)
Ol LLD (Eq. 1c)
C
Ni in whole rock (ppm)
MgO in whole rock (wt. %)
Hawaii
MORB
Ol LLD1 (1b; H&T; 1500 Ni)
Ol LLD2 (1c; P08; 1500 Ni)
Ol LLD3 (1a; H&T; 1200 Ni)

Figure 7

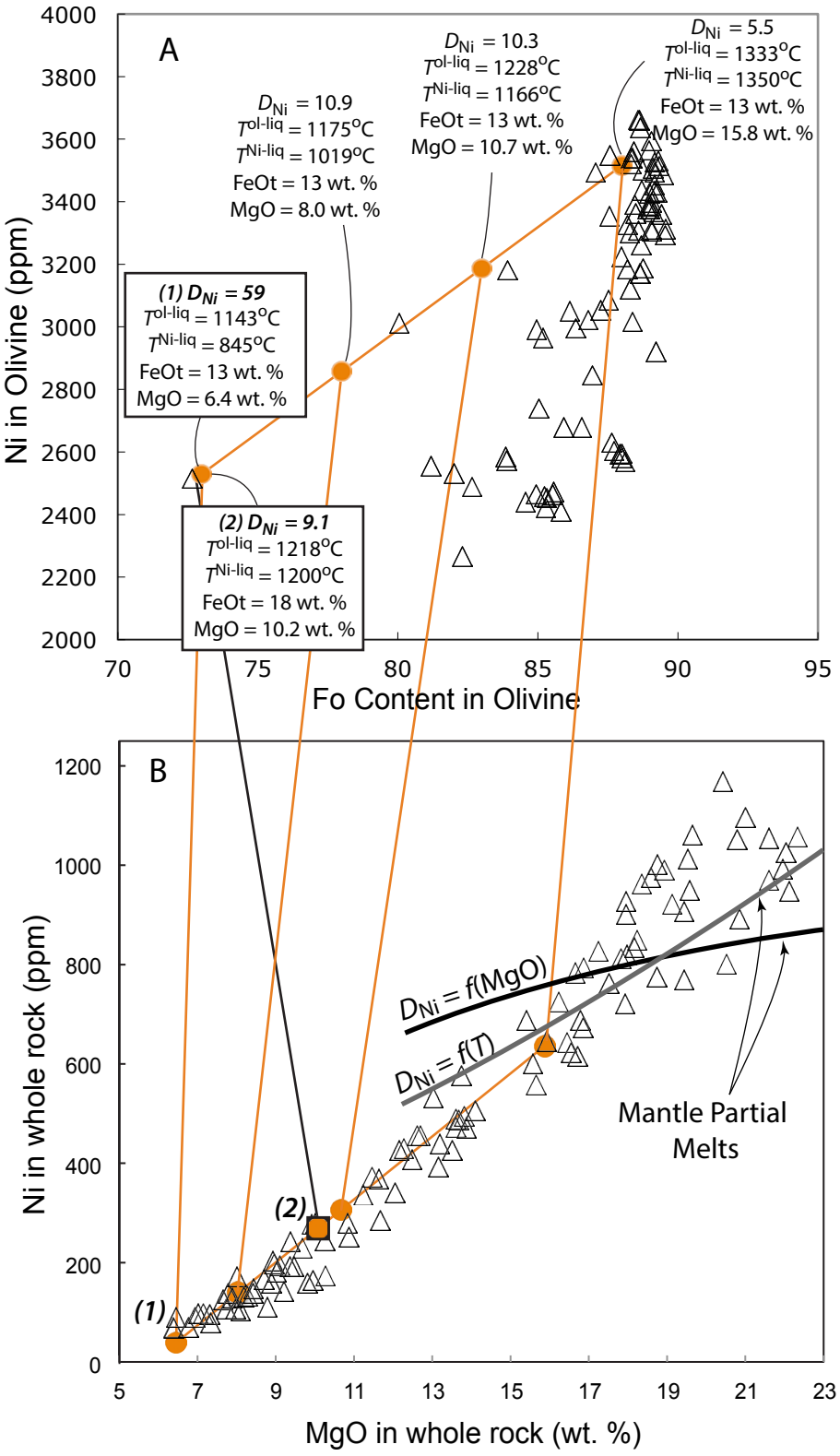
A
B
Ni in Olivine (ppm)
Fo Content in Olivine
Ni in whole rock (ppm)
MgO in whole rock (wt. %)
D_{Ni} = 10.9
T^{ol-liq} = 1175°C
T^{Ni-liq} = 1019°C
FeOt = 13 wt. %
MgO = 8.0 wt. %
D_{Ni} = 10.3
T^{ol-liq} = 1228°C
T^{Ni-liq} = 1166°C
FeOt = 13 wt. %
MgO = 10.7 wt. %
D_{Ni} = 5.5
T^{ol-liq} = 1333°C
T^{Ni-liq} = 1350°C
FeOt = 13 wt. %
MgO = 15.8 wt. %
(1) D_{Ni} = 59
T^{ol-liq} = 1143°C
T^{Ni-liq} = 845°C
FeOt = 13 wt. %
MgO = 6.4 wt. %
(2) D_{Ni} = 9.1
T^{ol-liq} = 1218°C
T^{Ni-liq} = 1200°C
FeOt = 18 wt. %
MgO = 10.2 wt. %
D_{Ni} = f(MgO)
D_{Ni} = f(T)
Mantle Partial Melts
(1)
(2)

Figure 8

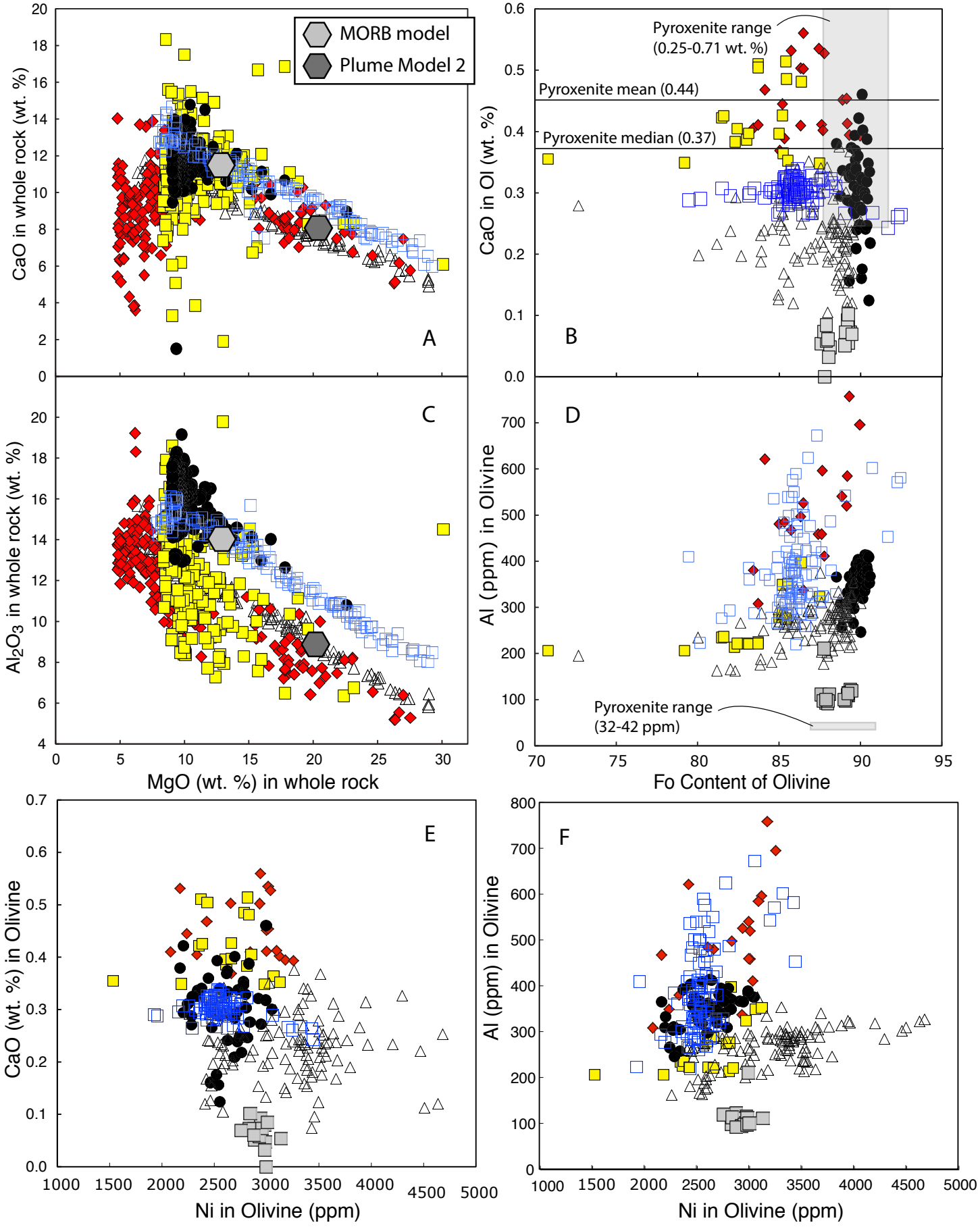
MORB model
Plume Model 2
CaO in whole rock (wt. %)
A
Pyroxenite range
(0.25-0.71 wt. %)
Pyroxenite mean (0.44)
Pyroxenite median (0.37)
CaO in Ol (wt. %)
B
Al2O3 in whole rock (wt. %)
C
MgO (wt. %) in whole rock
D
Al (ppm) in Olivine
Pyroxenite range
(32-42 ppm)
Fo Content of Olivine
E
CaO (wt. %) in Olivine
Ni in Olivine (ppm)
F
Al (ppm) in Olivine
Ni in Olivine (ppm)

Figure 9

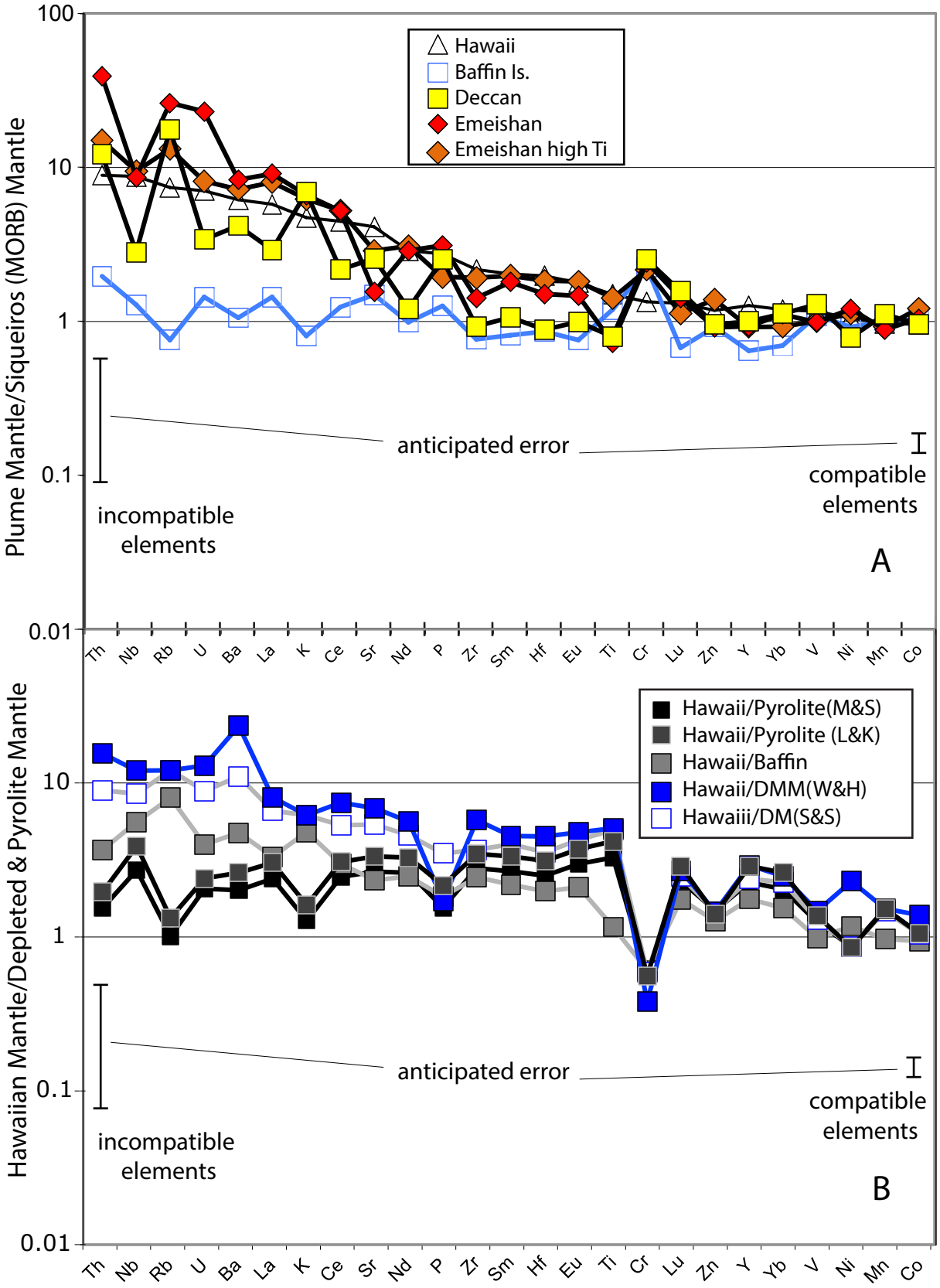
Plume Mantle/Siqueiros (MORB) Mantle
100
10
1
0.1
0.01
Hawaii
Baffin Is.
Deccan
Emeishan
Emeishan high Ti
anticipated error
incompatible elements
compatible elements
A
Th Nb Rb U Ba La K Ce Sr Nd P Zr Sm Hf Eu Ti Cr Lu Zn Y Yb V Ni Mn Co
Hawaiian Mantle/Depleted & Pyrolite Mantle
Hawaii/Pyrolite(M&S)
Hawaii/Pyrolite (L&K)
Hawaii/Baffin
Hawaii/DMM(W&H)
Hawaiii/DM(S&S)
anticipated error
incompatible elements
compatible elements
B
Th Nb Rb U Ba La K Ce Sr Nd P Zr Sm Hf Eu Ti Cr Lu Zn Y Yb V Ni Mn Co

Figure 10

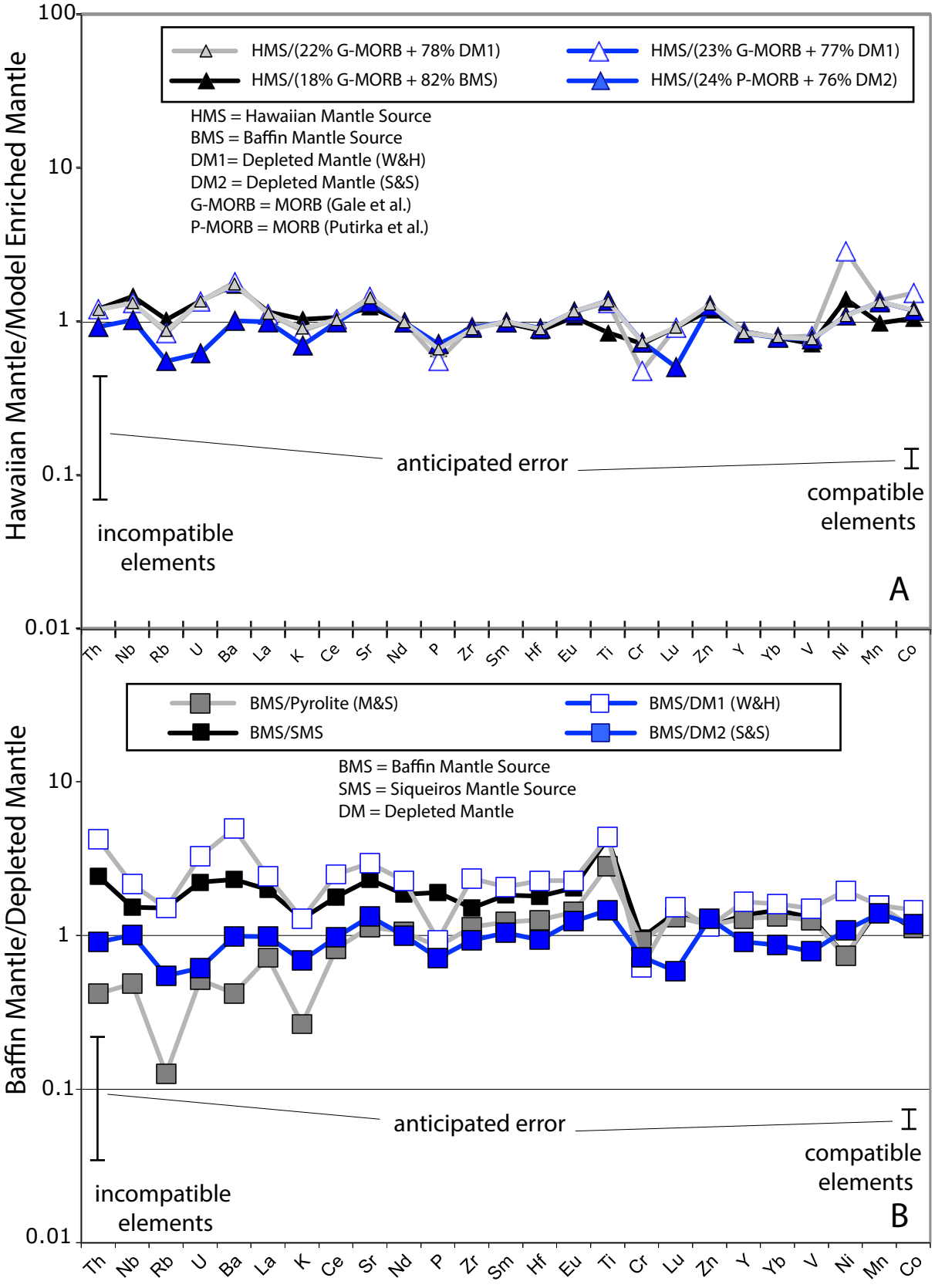
HMS/(22% G-MORB + 78% DM1)
HMS/(23% G-MORB + 77% DM1)
HMS/(18% G-MORB + 82% BMS)
HMS/(24% P-MORB + 76% DM2)
HMS = Hawaiian Mantle Source
BMS = Baffin Mantle Source
DM1= Depleted Mantle (W&H)
DM2 = Depleted Mantle (S&S)
G-MORB = MORB (Gale et al.)
P-MORB = MORB (Putirka et al.)
Hawaiian Mantle/Model Enriched Mantle
100
10
1
0.1
0.01
anticipated error
incompatible elements
compatible elements
A
Th Nb Rb U Ba La K Ce Sr Nd P Zr Sm Hf Eu Ti Cr Lu Zn Y Yb V Ni Mn Co
BMS/Pyrolite (M&S)
BMS/DM1 (W&H)
BMS/SMS
BMS/DM2 (S&S)
BMS = Baffin Mantle Source
SMS = Siqueiros Mantle Source
DM = Depleted Mantle
Baffin Mantle/Depleted Mantle
10
1
0.1
0.01
anticipated error
incompatible elements
compatible elements
B
Th Nb Rb U Ba La K Ce Sr Nd P Zr Sm Hf Eu Ti Cr Lu Zn Y Yb V Ni Mn Co

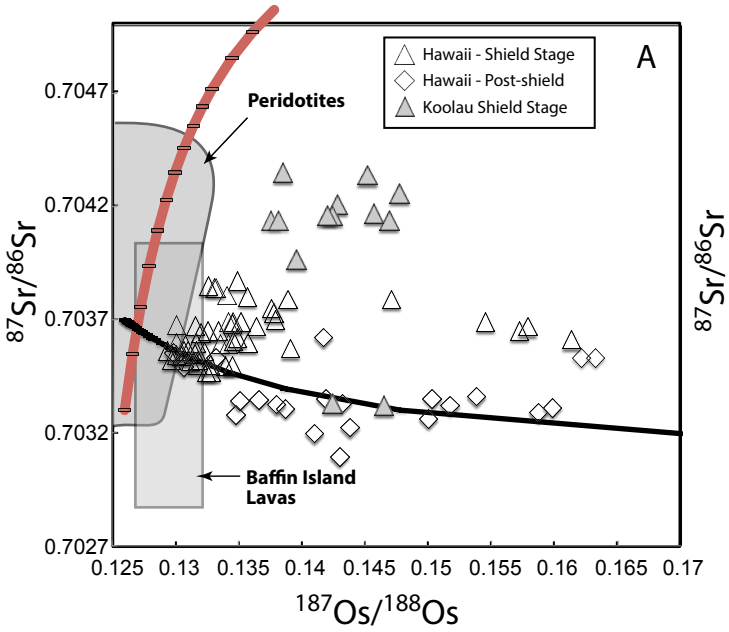

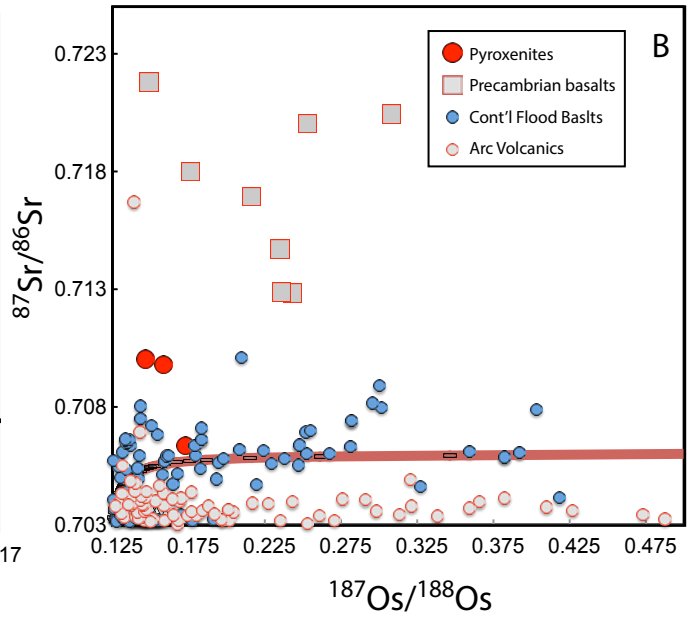

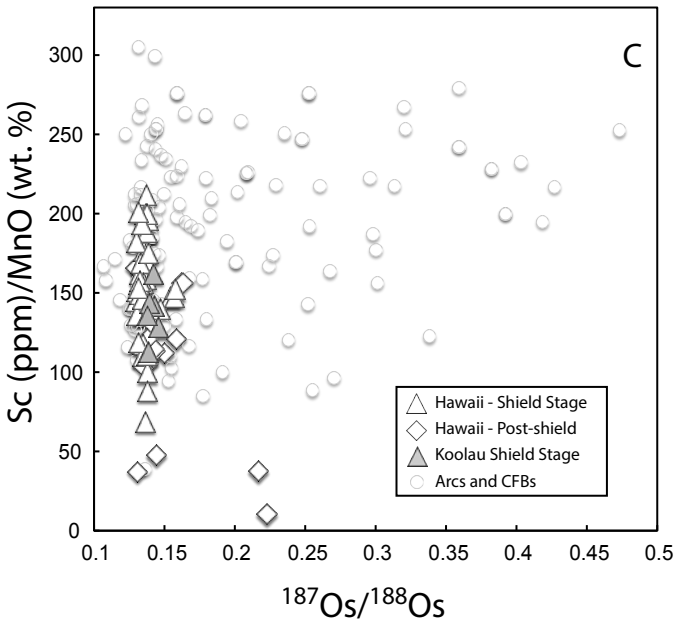

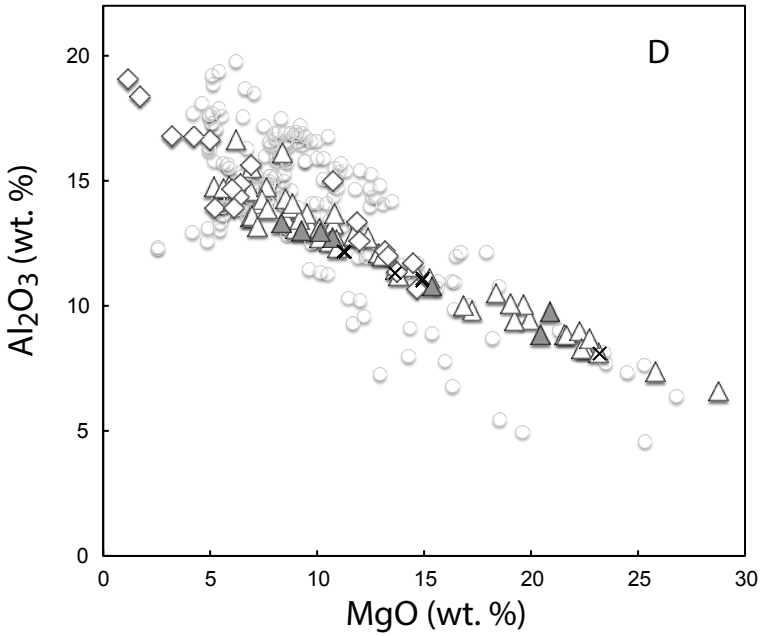

Figure ES1. $^{87}Sr/^{86}Sr$ vs. $^{187}Os/^{188}Os$ ratios for (A) Hawaiian shield stage and post-shield lavas, with shield stage Koolau lavas highlighted; also shown are fields for peridotites and lavas from Baffin Island, and (B) Arc lavas, Continental Food Basalts, Pyroxenites, and Precambrian lavas. Orange curves show mixing between the Kogiso et al. (2004) components of peridotite ($^{87}Sr/^{86}Sr$ = 0.7033, [Sr] = 10 ppm, $^{187}Os/^{188}Os$ = 0.126, and [Os] = 300 ppt), and a pyroxenite ($^{87}Sr/^{86}Sr$ = 0.706, [Sr] = 100 ppm, $^{187}Os/^{188}Os$ = 2, and [Os] = 10 ppt). The black curves shows mixing between this same periodtite source, and a hypothetical source similar to the pyroxenite, but with $^{87}Sr/^{86}Sr$ = 0.702 ([Sr] = 100 ppm,$^{187}Os/^{188}Os$ = 2, and [Os] = 10 ppt). In (C), $^{187}Os/^{188}Os$ is compared to Sc/MnO, which should be either fractionated by pyroxene- or garnet-rich source materials. And in (D) we see that Al_2O_3 contents are not any higher, relative to degree of fractionation (MgO) for Hawaiian lavas with elevated $^{187}Os/^{188}Os$. These plots collectively show that a pyroxenite source, or any ancient source material, is an unlikely candidate for high $^{187}Os/^{188}Os$ ratios, as these would likely have much greater $^{87}Sr/^{86}Sr$ than supposed by Kogiso et al. (2004), and because there is no distinctive mineralogic signal with respect to major oxides or trace elements. An intriguing pattern is that CFBs and arcs are both enriched in $^{187}Os/^{188}Os$ with CFBs ranging to higher $^{87}Sr/^{86}Sr$, and with Hawaiian lavas sharing a muted arc-like $^{187}Os/^{186}Os$ enrichment. These patterns point to a shallow source for high $^{187}Os/^{188}Os$, one that may be driven by assimilation/mixing processes, with a crustal influence for CFBs (and so their elevated $^{87}Sr/^{86}Sr$), but not so (or much less so) for oceanic islands and arcs.